Neurobiology of Disease 146 (2020) 105140

Contents lists available at ScienceDirect

Neurobiology of Disease

journal homepage: www.elsevier.com/locate/ynbdi

RUES2 hESCs exhibit MGE-biased neuronal differentiation and muHTT-dependent defective specification hinting at SP1

Paola Conforti[a,b], Dario Besusso[a,b], Silvia Brocchetti[a,b], Ilaria Campus[a,b], Claudio Cappadona[a,b], Maura Galimberti[a,b], Angela Laporta[a], Raffaele Iennaco[a,b], Riccardo L. Rossi[b], Vittoria Bocchi Dickinson[a,b], Elena Cattaneo[a,b,*]

[a] Laboratory of Stem Cell Biology and Pharmacology of Neurodegenerative Diseases, Department of Biosciences, University of Milan, 20122 Milan, Italy
[b] Istituto Nazionale Genetica Molecolare, Romeo ed Enrica Invernizzi, Milan 20122, Italy

ARTICLE INFO

Keywords:
Huntington's disease
Pluripotent stem cell
Isogenic cell lines
Neurodegeneration
Striatal differentiation
Neuronal specification
SP1

ABSTRACT

RUES2 cell lines represent the first collection of isogenic human embryonic stem cells (hESCs) carrying different pathological CAG lengths in the HTT gene. However, their neuronal differentiation potential has yet to be thoroughly evaluated. Here, we report that RUES2 during ventral telencephalic differentiation is biased towards medial ganglionic eminence (MGE). We also show that HD-RUES2 cells exhibit an altered MGE transcriptional signature in addition to recapitulating known HD phenotypes, with reduced expression of the neurodevelopmental regulators NEUROD1 and BDNF and increased cleavage of synaptically enriched N-cadherin. Finally, we identified the transcription factor SP1 as a common potential detrimental co-partner of muHTT by *de novo* motif discovery analysis on the LGE, MGE, and cortical genes differentially expressed in HD human pluripotent stem cells in our and additional datasets. Taken together, these observations suggest a broad deleterious effect of muHTT in the early phases of neuronal development that may unfold through its altered interaction with SP1.

1. Introduction

For many years after the discovery of the abnormally elongated CAG trinucleotides in the huntingtin gene (*HTT*), resulting in a poly-glutamine (polyQ) stretch in the HTT protein, as the genetic cause of Huntington's disease (HD), the pathogenesis was studied primarily in vivo using genetic models (Farshim and Bates, 2018). These studies provided valuable information on how mutant HTT (muHTT) causes progressive degeneration of the medium-spiny striatal neurons (MSNs), in addition to the dysfunction and progressive loss of neurons in the cerebral cortex. Mutant HTT is known to form intracellular oligomers and aggregates, and is thought to have a toxic gain-of-function that interferes with many cellular and biological processes (Rataj-Baniowska et al., 2015), causing transcriptional, metabolic, and axonal transport defects and excitoxicity in neurons. Glial cell function is also affected (Osipovitch et al., 2019). The mutation in CAG repeat length varies in patients, with longer CAG repeats correlating with earlier HD onset (Gusella and MacDonald, 2006; Lee et al., 2012a, 2012b). Accordingly, in an attempt to recapitulate this correlation between the pathological CAG sizes and the clinical symptoms observed in patients, knock-in genetic models have been generated by inserting a progressively increasing CAG repeat, ranging from 50 (White et al., 1997) to 150 (Lin et al., 2001), in the endogenous HTT gene. Knock-in models develop behavioral deficits at a very early age, even before neuropathology, though none of these models exhibit neuronal death or gliosis, even in very old mice (Lucas and Ortega, 2011). These results demonstrate that neuronal dysfunction precedes neuronal death, which is in agreement with the presence of subtle clinical symptoms and cortical thinning in HD patients decades before the appearance of relevant motor signs (Nanetti et al., 2018; Sampedro et al., 2019; Smith et al., 2000).

The advent of human pluripotent stem cell (hPSC) technologies and neuronal differentiation methods have added valuable information to HD research. Disease-relevant human MSNs and cortical neurons can be obtained from hPSCs carrying different sizes of CAG repeats in *HTT* exon 1 and used to identify disease-perturbed regulatory networks during the course of neuronal differentiation *in vitro* and in mature neurons. Some studies have employed patient-derived human induced pluripotent stem cells (hiPSCs), which have the advantage of carrying

* Corresponding author at: Laboratory of Stem Cell Biology and Pharmacology of Neurodegenerative Diseases, Department of Biosciences, University of Milan, 20122 Milan, Italy.
E-mail address: elena.cattaneo@unimi.it (E. Cattaneo).

https://doi.org/10.1016/j.nbd.2020.105140
Received 18 August 2020; Received in revised form 9 October 2020; Accepted 11 October 2020
Available online 13 October 2020

the mutation in the context of the genome of the donor in association with the corresponding clinical information. Another relevant cell model is represented by an engineered allelic series of isogenic human embryonic stem cell (hESC) lines carrying a gradual increase in CAG repeat length (Ruzo et al., 2018). Common evidence from all of these studies is the demonstration that hPSCs carrying the HD mutation exhibit early neuronal defects. In particular, one study found that the expanded CAG negatively impacts the transition from the pluripotent stem cell state to neuroectoderm, as well as the formation of polarized neuroepithelial structures (Conforti et al., 2018). In other studies, neuruloid morphogenesis (Haremaki et al., 2019) and cytokinesis (Ruzo et al., 2018) were severely affected, with giant cells appearing in the dish and resulting in developmental delay. Altered neuronal gene transcription, electrophysiology, metabolism, and cleavage of critical cell adhesion molecules that are enriched in synapses (e.g., N-cadherin, NCAD) have also been reported, consistent with impaired neurogenesis (Conforti et al., 2018; HD iPSC Consortium, 2012, 2017). Defects in the differentiation of MSNs, cortical progenitor homeostasis and cytoarchitecture in 3D organoids (Conforti et al., 2018), and transcriptional alterations in HD cortical neurons have also been described (Mehta et al., 2018). These data indicate that the expression of muHTT in human cells exposed to cortical and striatal differentiation protocols causes delayed maturation and altered morphology of several neuronal subtypes, implying early abnormalities of neurological development, at least in vitro. Such impaired neurological development would compromise neuronal homeostasis in adulthood, leading to greater cellular vulnerability to advanced life stressors (Ramocki and Zoghbi, 2008).

Evidence mostly from animal models indicates that HTT has multiple roles during neurogenesis; therefore, its mutation may cause dysfunctions, starting during embryogenesis (Godin et al., 2010; Lopes et al., 2016; HD iPSC Consortium, 2012; Molero et al., 2009, 2016). Furthermore, expression of polyQ-expanded HTT up to postnatal day 21 in mice has been found to recapitulate some of the typical biochemical and behavioral HD symptoms observed in animals expressing muHTT throughout life (Molero et al., 2009, 2016). The possibility of altered brain development is also suggested by evidence of a smaller intracranial brain volume (Nopoulos et al., 2011) and smaller head size (Lee et al., 2012a) in HD carriers decades before predicted motor onset. This possibility seems to find support in a recent study that compared tissue fragments from control and HD human fetal brains of various ages and concluded in favor of abnormal neuronal development, though the scarcity of data and lack of relevant evidence from HD samples raises some concerns (Barnat et al., 2020). Detailed analysis of cells and recognizable brain tissue is indispensable for establishing whether the basic mechanisms of neural development are altered in the presence of an HD mutation. In this context, hPSCs carrying the HD mutation and exposed to neuronal differentiation can help paint the picture.

Here, we report that, upon exposure to a striatal differentiation protocol (Delli Carri et al., 2013), the hESC line H9 and hiPSC line KOLF2 up-regulate markers of the lateral ganglionic eminences (LGE), the brain region that gives rise to the MSNs of the striatum during development, whereas the RUES2 parental line acquires a significantly more ventralized identity, as indicated by up-regulation of medial ganglionic eminence (MGE) transcripts. Presence of an expanded CAG in the RUES2 line negatively affects the MGE transcriptional signature, as well as levels of other neurodevelopment transcripts, including BDNF. These data, together with the literature, show that the detrimental effect of muHTT in hPSC differentiation is not lineage-specific, but affects multiple neuronal types. *In silico* analysis highlighted transcription factor (TF) SP1 as a potential common co-partner of adverse muHTT activity during neuronal differentiation. Taken together, these observations suggest a broad deleterious effect of muHTT during the early stages of neuronal development that may unfold through its altered interaction with SP1.

2. Material and methods

2.1. Human cell cultures

RUES2 hESC lines derived and kindly provided by Prof. Ali Brinvalou's Laboratory (Rockefeller University) and H9 hESCs (WiCell Research Institute) were cultured in mTeSR1 (Supplement Fig. 1A). Proliferating RUES2 cells grew in adhesion on Geltrex™ (Thermo Fisher Scientific), whereas H9 cells were maintained on Cultrex coated plates (Trevigen). KOLF2 hiPSCs were kindly provided by the Sanger Institute's Human Induced Pluripotent Stem Cell Initiative (HipSci) project. Pluripotent KOLF2 cells were grown in TeSR-E8 (Voden) on tissue culture plates coated with Synthemax II-SC substrate (Corning) under feeder-free conditions (Supplement Fig. 1A). Additional control (Q21n1) and HD (Q60n5, Q109n1) hiPSCs generated and characterized in previous studies (HD iPSC Consortium, 2017; Conforti et al., 2018) were cultured in mTESR1 medium (Voden) and plated on Cultrex (Trevigen).

All cell lines used in this study were maintained under sterile conditions and regularly tested for mycoplasma (Eurofins). The karyotype of each line/clone was monitored every 3 months by Q-banding analysis (ISENET).

2.2. Striatal differentiation

HD and control hPSC lines were exposed to the striatal differentiation protocol published by Delli Carri et al. (2013). Briefly, cells were plated at a density of 0.6×10^5 cells/cm^2 on Cultrex-coated plates (120–180 μg/ml) in complete mTeSRTM1 medium and expanded for 2 days. When cultures reached 70% confluence, cells were exposed to neural induction medium [DMEM-F12 (Gibco), N2 supplement (Gibco), B-27 without retinoic acid (Gibco), 10 μM SB431542, and 500 nM LDN193189] for 12 days. Neural induction lasts 12 days and is triggered by the dual SMAD inhibitor compounds SB431542 (a blocker of the TGF-β pathway) and LDN193189 (an inhibitor of the BMP pathway) (Chambers et al., 2009). These two reagents were provided by CHDI Foundation (NY, USA). Patterning and specification of the cells towards the ventral telencephalic fate lasts from day 5 to day 25. In this time window 200 ng/ml recombinant human SHH (PrepoTech) and 100 ng/ml DKK-1 (PrepoTech) were added. At DIV15, cells were detached by Accutase single cell dissociation and replated at a density of 2.5×10^4 cells/cm^2 on Matrigel-coated plates (240–360 μg/ml). Neuronal maturation lasts from day 25 to day 50 and is achieved in the presence of 30 ng/ml BDNF (PrepoTech,) in DMEM-F12 plus N-2 and B-27 supplements (Gibco).

2.3. Western blot

At specific time points of differentiation, cell cultures were collected and lysed in RIPA buffer (50 mM Tris-HCl pH 8, 150 mM NaCl, 0.1% SDS, 1% NP40) supplemented with 1 mM PMSF and Halt Protease & Phosphatase Inhibitor Cocktail (Thermo Scientific). The protein concentration was determined using the Pierce BCA Protein Assay Kit (Thermo Scientific). Equal amounts of total proteins were loaded on 7.5% or 10% SDS-PAGE gels and transferred to a nitrocellulose membrane (Bio-Rad) using the Trans-Blot® Turbo™ System (Bio-Rad). Membranes were blocked for 1 h at room temperature (RT) in 0.1% TBS-T with 5% non-fat dry milk (Bio-Rad) and incubated overnight at 4 °C with the following primary antibodies: MAP2a/b (mouse, 1:500; Beckton Dickinson), CTIP2 (rat, 1:500; Abcam), GAD67 (mouse, 1:1000; Millipore), DARPP32 (rabbit, 1:500; Abcam), N-CAD (mouse, 1:500; Beckton Dickinson), and ADAM10 (rabbit, 1:1000; Abcam). Membranes were washed thrice in 0.1% TBS-T and incubated for 1 h at RT with the appropriate HRP-I conjugated secondary antibodies (dilution 1:3000, Bio-Rad). Following three washes, immunoreactive bands

were detected using Clarity™ western ECL Substrate (Bio-Rad) in accordance with the manufacturer's instructions. GAPDH (rabbit, 1:5000; Abcam) was used to normalize expression. Acquisitions were performed using a ChemiDoc MP imaging system (Bio-Rad) and densitometric analysis using ImageLab software.

2.4. Immunocytochemistry

Cell cultures were fixed with ice-cold 4% paraformaldehyde for 15 min and washed thrice with phosphate-buffered saline (PBS) at specific times. Next, cells were permeabilized with 0.5% Triton X-100 in PBS for 10 min and subsequently blocked with 5% normal goat serum (NGS, Vector) for 1 h at RT. Cells were incubated overnight at 4 °C with primary antibodies diluted in solution containing 2.5% NGS and 0.25% Triton X-100. Appropriate Alexa Fluor®-conjugated secondary antibodies (Molecular Probe, Life Technologies) were diluted 1:500 in PBS and mixed with 0.1 μg/ml Hoechst (Invitrogen) to counterstain the nuclei. Images were acquired on a Leica TCS SP5 Confocal Laser Scanning Microscope (Leica Microsystems) using a 40× oil immersion objective with a zoom of 1.7. CellProfiler software (version 2.1.1) was used to quantify positive cells.

The following primary antibodies were used: OCT3/4 (mouse, 1:100; Santa Cruz), Ki67 (rabbit, 1:500; Abcam), p27 (mouse, 1:1000; Cell Signaling), PALS1 (rabbit, 1:500; Cell Signaling), N-CAD (mouse, 1:800; Beckton Dickinson), GSX2 (rabbit, 1:250; Millipore), ASCL1 (mouse, 1:1000; Beckton Dickinson), FOXG1 (rabbit, 1:1000; Diatech), NKX2.1/TTF1 (rabbit, 1:2500; Abcam), CTIP2 (rat, 1:1000; Abcam), DARPP32 (rabbit, 1:250; Abcam), TBR1 (rabbit, 1:1000; Abcam), TBR2 (rabbit, 1:1000; Abcam).

2.5. Real-time qPCR and biomark analysis

RNA was prepared using Trizol reagent according to the manufacturer's instructions (Thermo Fisher Scientific). After treating RNA with the DNA-free Kit (Ambion, Invitrogen) to remove contaminating DNA, 500 μg RNA was retrotranscribed using the iScript cDNA Synthesis Kit (Bio-Rad). Conventional qPCR was performed in a 15 μl volume containing 50 ng cDNA and SsoFast™ EvaGreen® Supermix 2× (Bio-Rad) in a CFX96 Real-Time System (Bio-Rad). Gene expression analysis was performed using this method for the BDNF total transcript (forward: 5′-TAACGGCGGCAGACAAAAAGA-3′; reverse: 5′-GAAGTATTGCTTCA GTTGGCCT-3′) and reference gene 18S (forward: 5'-CGGCTACCACAT CCAAGGAA-3′; reverse: 5'-GCTGGAATTACCGCGGCT-3′).

All other gene expression analyses were carried out using Fluidigm 96.96 dynamic arrays (Fluidigm Corporation, CA, USA) according to the manufacturer's instructions. Pre-amplification reactions were prepared by mixing PreAmp Master Mix, the pooled TaqMan assay 0.2×, and nuclease-free water. The panel of all TaqMan probes is reported in Supplementary Table 2. Briefly, for each sample, 3.75 μl of PreAmp Mix was aliquoted in a 96-well PCR plate and 1.25 μl of newly retrotranscribed cDNA added to reach a total volume of 5 μl. The pre-amplification was performed in a GeneAmp PCR System 9700 (Applied Biosystems). The 96.96 dynamic array IFC Chips (Fluidigm) were primed with the IFC controller fluid (Fluidigm). After priming, the dynamic array was loaded with 5 μl of each assay and sample mix into the appropriate inlets of the primed chip and loaded with the IFC controller. After loading, the chip was placed in the Biomark instrument and qPCR performed.

2.6. De novo motif discovery analysis

The gene IDs (obtained from NCBI) of the selected genes were submitted to RSAT retrieve sequences (http://rsat.sb-roscoff.fr/retrieve-seq_form.cgi) to obtain the 3000 bp upstream the genes. The searching parameters were set as follows: in mandatory options “Single Organism_ *Homo sapiens* GRCh38, in advanced options “Prevent overlap” unselected and “Mask repeats” selected. Then, the output was loaded in two *de novo* web accessible motif discovery tools: MEME (http://meme-suite.org/tools/meme) and RSAT Oligo Analysis (http://rsat.sb-roscoff.fr/retrieve-seq_form.cgi). MEME parameters were set as follow: the number of motifs that MEME should find was set to 12, the background was set to 1st order model of sequences, minimum width of 6 and maximum width of 12, the other parameters were as default. Oligo Analysis parameters were: *H. sapiens* was selected as organism, the estimate from input sequence was set to Markov model (higher order of dependencies) order 2, max matrices 12, min site weight 6. The motifs identified were submitted to STAMP (http://www.benoslab.pitt.edu/stamp/) to identify the 10 best matches to each of the discovered motif in JASPAR v2010 and TRANSFAC v11.3 databases.

The motifs identified in the 4 different output (MEME_JASPAR, MEME_TRANSFAC, Oligo_JASPAR, Oligo_TRANSFAC) were compared and only the TFs represented in at least 2 different motif discovery tools with high score were considered. Each predicted TFs was examined looking for literature evidences in respect to the biological role and disease context. To further investigate and confirm the predicted interactions we submitted the list of the genes of a specific area (i.e LGE) and the respective TFs found to public pathway and interactions database Pathway Commons (https://www.pathwaycommons.org). Many interactions were confirmed, and the networks obtained were imported in Cytoscape 3.7.1 (http://cytoscape.org/) and enriched with the predicted interactions.

2.7. Statistical analysis

All statistical analyses were performed using Prism (GraphPad Software). One-way ANOVA with Tukey's post-hoc test was performed for all biological experiments including HD and control lines. Student *t*-test was used to compare only two group conditions. The numbers in each individual experiment and tests used are described in the figure legends. $P < 0.05$ was considered significant.

3. Results

3.1. Diverse hPSC lines present different propensities to respond to a striatal MSN differentiation protocol

To investigate the neuronal differentiation potential of the parental RUES2 line and, subsequently, its HD derivatives, we exposed cells to a stepwise striatal differentiation protocol that mimics human ventral telencephalon development (Delli Carri et al., 2013; Onorati et al., 2014) (Fig. S1A), together with H9 and KOLF2 cell lines (clone C1; Fig. S1B). These three cell lines all exhibited a normal karyotype (Fig. S1C).

First, we compared the H9 and RUES2 cell proliferative state by evaluating the proportion of $Ki67^+$ and $p27^+$ cells at DIV0, 15, 25, and 50 (Figs. 1A, B). The percentage of $Ki67^+$ cells decreased over time with an increase in $p27^+$ post-mitotic neurons, suggesting that both lines exited the cell cycle (Figs. 1C, D) and acquired neuronal morphologies with similar timing (Fig. 1A and S1D). Next, we investigated the ability of the lines to acquire a striatal-MSN cell identity. Similar levels of telencephalic marker FOXG1 were found in both lines at DIV15 (Figs. 1E, F). In contrast, when counting the number of GSX2 and ASCL1-positive cells at DIV25, the RUES2 culture was significantly reduced in GSX2 or ASCL1-positive and $GSX2^+/ASCL1^+$ double-positive progenitors (Figs. 1G, H). Co-expression of CTIP2 with DARPP32 qualifies cells *in vitro* as being bona-fide MSNs (Besusso et al., 2020). Immunocytochemistry and cell counting revealed that RUES2 cells did not express DARPP32 at the end of the differentiation, as indicated by the absence of $CTIP2^+/DARPP32^+$ neurons (Figs. 1I, J). Western blot analysis further confirmed this observation. Although the RUES2 line behaved similar to the H9 line in terms of MAP2, CTIP2, and GAD67 protein levels, DARPP32 was almost undetectable at the end of differentiation (Figs. 1K, L and S1E). The KOLF2 hiPS line exposed to the

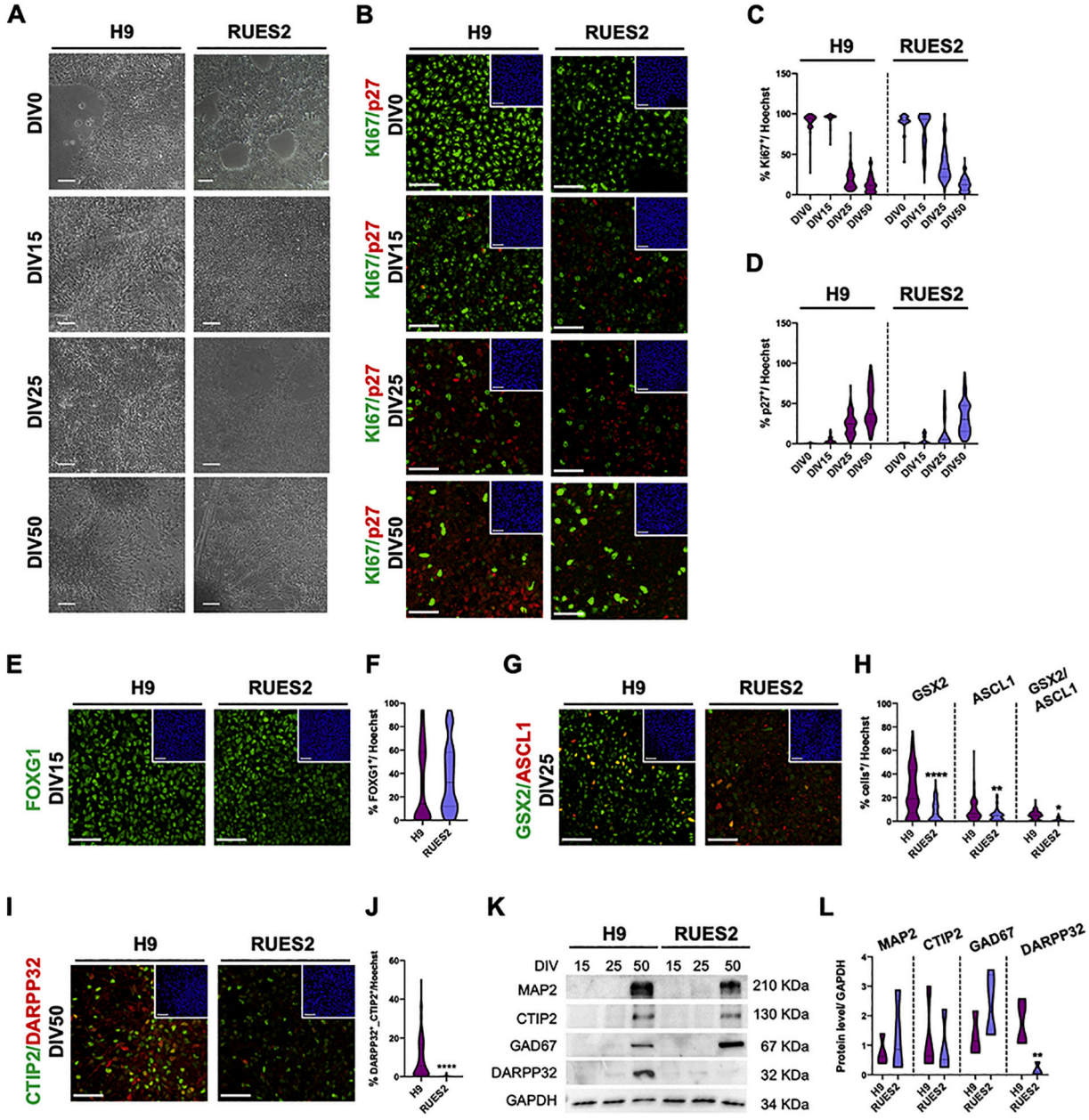

Fig. 1. Different hPSC lines present different propensities to respond to striatal differentiation.

(A) Cell morphology of the H9 and RUES2 lines was monitored during differentiation (DIV0, DIV15, DIV25, and DIV50) by phase contrast microscopy. Representative phase contrast images (4× objective) are shown for each time point with an additional 10× objective image at DIV50 to highlight the presence of neurite outgrowth, neurofilaments, and processes from cell bodies at the end of differentiation. Scale bar, 200 µm.

(B) Immunocytochemistry of Ki67 and p27 at DIV0, DIV15, DIV25, and DIV50 of differentiation for the H9 and RUES2 lines. Scale bar, 50 µm. Top right, Hoechst inset.

(C-D) Counts of $Ki67^+$ and $p27^+$ cells for the H9 and RUES2 lines by CellProfiler software (version 2.1.1). $N = 4$ biological replicates for H9 and $N = 3$ for RUES2.

(E) Immunocytochemistry of FOXG1 at DIV15 of differentiation for the H9 and RUES2 lines. Scale bar, 50 µm. Top right, Hoechst inset.

(F) Counts of $FOXG1^+$ cells for the H9 and RUES2 lines by CellProfiler software (version 2.1.1). N = 4 biological replicates for H9 and $N = 3$ for RUES2.

(G) Immunocytochemistry of GSX2 and ASCL1 at DIV25 for the H9 and RUES2 lines. Scale bar, 50 µm. Top right, Hoechst inset.

(H) Counts of $GSX2^+$, $ASCL1^+$, and $GSX2^+/ASCL1^+$ cells for the H9 and RUES2 lines by CellProfiler software (version 2.1.1). N = 4 biological replicates for H9 and $N = 3$ for RUES2. Data are presented as mean ± SEM (H9 $GSX2^+$ DIV25: 24.61% ± 1.73%, RUES2 DIV25: 8.6% ± 0.8%; $ASCL1^+$ DIV25: 9.19% ± 0.73%, RUES2 DIV25: 5.12% ± 0.45%; $GSX2^+/ASCL1^+$ DIV25: 4.85% ± 0.31%, RUES2 DIV25: 1.21% ± 0.13%) $^{****}p < 0.0001$, $^{**}p < 0.01$, $^{*}p < 0.05$ using Student *t*-test to compare the two group conditions.

(I) Immunocytochemistry of CTIP2 and DARPP32 at the end of differentiation for the H9 and RUES2 lines. Scale bar, 50 µm. Top right, Hoechst inset.

(J) Counts of double-positive neurons ($CTIP2^+/DARPP32^+$ cells) for the H9 and RUES2 lines by CellProfiler software (version 2.1.1). N = 4 biological replicates for H9 and $N = 3$ for RUES2. Data are presented as mean ± SEM (H9 $DARPP32^+$: 18.5% ± 0.11% and $CTIP2^+/DARPP32^+$ 9.46% ± 0.07%). $^{****}p < 0.0001$, Student t-test.

(K) Western Blot analysis of MAP2, CTIP2, GAD67, and DARPP32 at DIV15, DIV25, and DIV50 of differentiation for the H9 and RUES2 lines. MAP2, CTIP2, GAD67, and DARPP32 protein levels were normalized to GAPDH. $N = 3$ biological replicates.

(L) Violin plot representing the densitometric analysis performed on western blot results. N = 3 biological replicates. Student t-test was used to compare each group condition, $^{**}p < 0.01$.

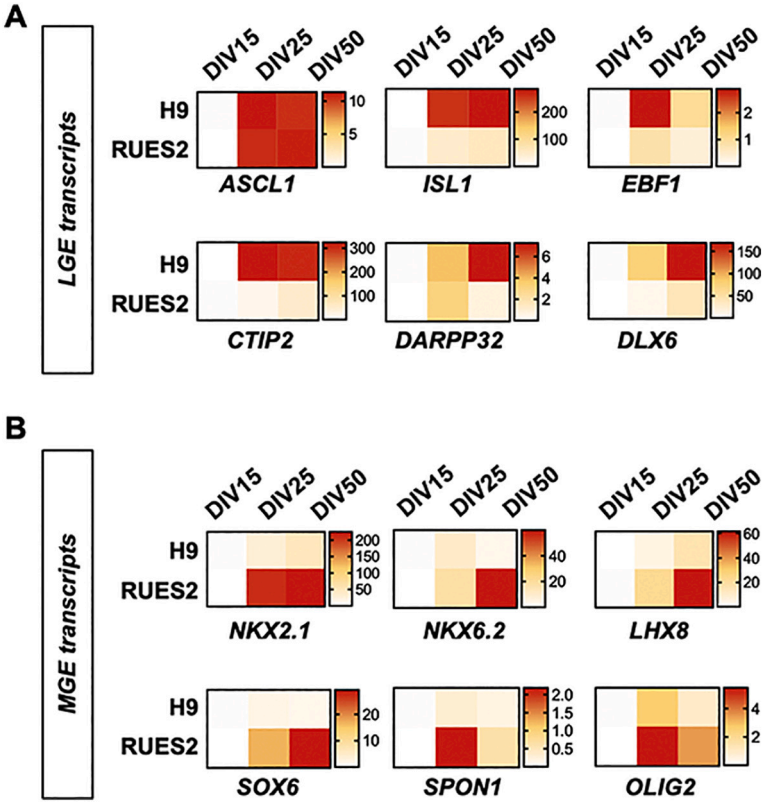

Fig. 2. RUES2 lines acquired an MGE-like profile after exposure to a striatal differentiation protocol.
(A) Heat map showing the expression levels in high-content qPCR analysis (Biomark) of the LGE at DIV15, DIV25, and DIV50 of the H9 and RUES2 lines. N = 3 biological replicates. *ISL1:* DIV25 $*p < 0.05$, DIV50 $**p < 0.01$; *EBF1:* DIV25 $**p < 0.01$; *CTIP2:* DIV25 $**p < 0.01$; *DARPP32:* DIV50 $***p < 0.001$; *DLX6:* DIV25 $**p < 0.01$, DIV50 $****p < 0.0001$, Student t-test. **(B)** Heat map showing the expression levels in high-content qPCR analysis (Biomark) of the MGE markers at DIV15, DIV25, and DIV50 of the H9 and RUES2 lines. N = 3 biological replicates. *NKX2.*1: DIV25 and DIV50 $****p < 0.0001$; *SOX6:* DIV25 $*p < 0.05$, DIV50 $****p < 0.0001$; *SPON1:* DIV25 $**p < 0.01$; *NKX6.2:* DIV50 $***p < 0.001$; *LHX8:* DIV50 $***p < 0.001$; *OLIG2:* DIV25 and DIV50 $*p < 0.05$, Student t-test.

same protocol was similar to H9 (Fig. S1F, G), as both $GSX2^+/ASCL1^+$ progenitors were present at DIV25 and $CTIP2^+/DARPP32^+/GAD67^+$ neurons were counted at the end of the protocol (Fig. S1G). DARPP32 and GAD67 were already detected at DIV25 of differentiation in the KOLF2 line (Fig. S1H, I). These data indicate that hPSC lines exhibit a distinct propensity to respond to the same ventral (striatal) differentiation protocol.

3.2. RUES2 line acquired an MGE-like expression profile after exposure to striatal differentiation

To investigate whether RUES2 and H9 lines are differentially specified along the dorso-ventral axis, we performed high-content qPCR analysis on select LGE and MGE markers from DIV15 to DIV50. Analysis of the ventral marker ASCL1 did not show any differential expression at the time points investigated (Fig. 2A; Fig. S2A, B). By monitoring the expression of LGE markers, we confirmed that H9 cells acquire an LGE cell fate through the progressive up-regulation of ISL1, EBF1, CTIP2, DARPP32, and DLX6 (Fig. 2A). The expression profile in differentiating H9 cells recapitulated the developmental transition from VZ to SVZ to mantle zone of the LGE as expected (Delli Carri et al., 2013). In contrast, this set of transcripts was significantly down-regulated in the RUES2 parental line at DIV50 (Fig. 2A; Fig. S2A). The RUES2 line acquired a more ventral MGE-like identity as indicated by the expression of the MGE transcripts NKX2.1, NKX6.2, LHX8, SOX6, SPON1 and OLIG2 (Fig. 2B). Of these mRNAs, NKX2.1, SOX6, and SPON1 were significantly up-regulated starting from DIV25, whereas NKX6.2, LHX8, and OLIG2 were significantly upregulated only at DIV50 (Fig. 2B; Fig. S2B).

In contrast to the H9 line, the RUES2 line did not exhibit any $TBR2^+/CTIP2^+$ and $TBR1^+/CTIP2^+$ cell populations typically associated with cortical development, further supporting the tendency of this line to acquire a more ventral identity (Fig. S3A, B). Gene expression analysis of the cortical markers TBR1, NEUROD1, and DATCH1 confirmed that these transcripts were all reduced in the RUES2 line compared to the H9 line (Fig. S3C). KOLF2 cells behaved similarly to H9 cells and expressed transcripts associated with MSN differentiation (Fig. S3D).

3.3. Changes in the SHH and WNT signaling pathways contribute to MGE regional identity

In humans, SHH and WNT signaling have opposite effects on regional specification of the ventral and dorsal telencephalon, respectively (Ma et al., 2019), whereas their combination sustains NKX2.1 expression, a transcript that is found in the MGE (Chi et al., 2016) and is up-regulated in differentiating RUES2 cells (Fig. 2B). Therefore, we looked at the main components of these signaling pathways in H9, RUES2, and KOLF2 cultures from DIV0 to DIV10. High-content gene expression analysis revealed no differences between the three cell lines in the mRNA levels of SHH (Fig. 3A; Fig. S4A), Indian Hedgehog (IHH), or the transmembrane protein Smoothened (SMO) (Fig. S4B). However, the RUES2 line presented significant up-regulation of the receptors of HH signaling, PTCH1 and PTCH2, and the transcriptional effectors GLI2 and GLI3 over H9 and KOLF2 cells (Fig. 3A; Fig. S4A), suggesting hyperactivation of SHH signaling in this line. (See Fig. 4.)

Acquisition of a ventral fate requires inhibition of dorsalizing WNT signaling. Therefore, we evaluated the expression of Dickkopf WNT Signaling Pathway Inhibitor 1 (DKK1), an inhibitor of WNT that is added to the medium starting from DIV5 to facilitate the acquisition of a ventral identity. As reported previously (Fasano et al., 2010), DKK1 expression peaked in H9 at DIV4, followed by progressive decline (Fig. 3B; Fig. S4A). In contrast, the RUES2 line maintained low levels of this transcript for the entire induction phase, whereas KOLF2 cells were similar to H9 cells (Fig. 3B). In addition, the RUES2 line exhibited a significant up-regulation of WNT ligands associated with the development of MGE interneurons, such as WNT1, WNT3A, and WNT5A (Chi et al., 2016; Zhang and Zhang, 2010) starting from DIV8 (Fig. 3B; Fig. S4A), whereas WNT8B, which is typically expressed in cortical neurons (Hasenpusch-Theil et al., 2017), was more highly expressed in H9 cells than RUES2 cells (Fig. S4C), supporting our previous analysis that the RUES2 line has a more ventralized identity than

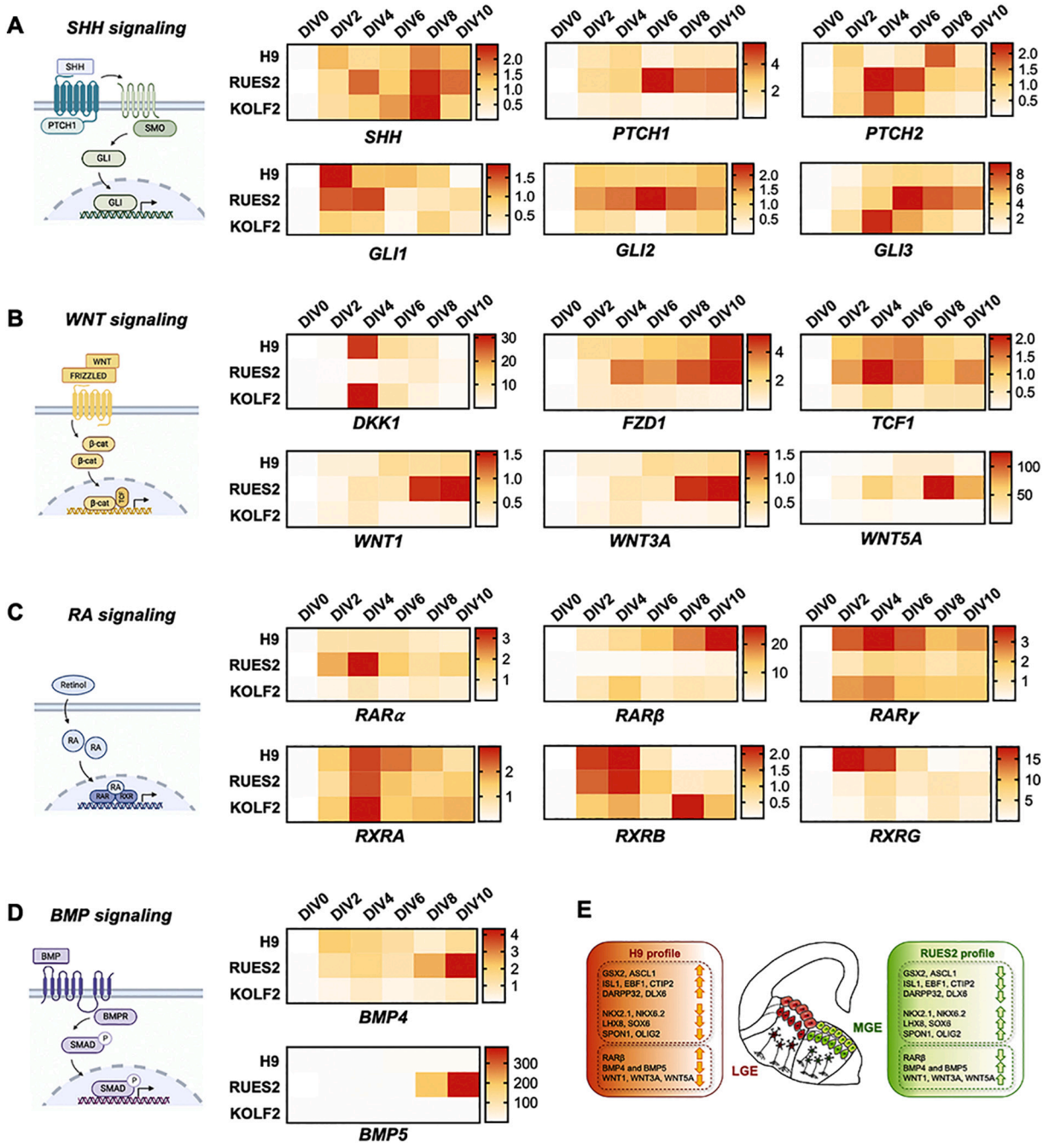

Fig. 3. Changes in the SHH and WNT signaling pathways contribute to defining MGE regional identity acquisition.
Summary diagram of signaling pathway components and heat map showing the expression levels in high-content qPCR analysis (Biomark) of **(A)** SHH, **(B)** WNT, **(C)** RA, and **(D)** BMP signaling components at DIV0, DIV2, DIV4, DIV6, DIV8, and DIV10 of differentiation of the H9, RUES2, and KOLF2-C1 lines. N = 3 biological replicates. H9 vs. RUES2, *PTCH1:* DIV6 **p < 0.01, *PTCH2:* DIV4 **p < 0.01, *DKK1:* DIV4 *p < 0.05, *WNT1:* DIV10 *p < 0.05, *WNT3A:* DIV10 **p < 0.01, *WNT5A:* DIV10 **p < 0.01; *RARB:* DIV10: ****p < 0.0001; *BMP4:* DIV10 *p < 0.05, *BMP5:* DIV10 *p < 0.05, one-way ANOVA with Tukey's post-hoc test.
(E) Schematic representation of the expression profile characteristics of the H9 and RUES2 lines with respect to the LGE, MGE, and signaling transcripts analyzed by high-content gene expression analysis.

the H9 line (Fig. 2B). Although we observed different profiles in the expression of WNT receptors FZD1, FZD2, FZD3 and intracellular signaling TCF1 from DIV0 to DIV10, no significant differences were found between the H9 and RUES2 parental lines at any time-points (Figs. 3B and S4C).

LGE-derived GABAergic neurons in the basal ganglia require retinoic acid for their development (Chatzi et al., 2011; Rataj-Baniowska et al., 2015). Therefore, we measured the expression of retinoic acid receptors RAR and RXR in all cell lines during neural induction. Though the mRNA levels of RARα, RARγ, and RXR did not differ between the RUES2 and H9 lines, RARβ was significantly reduced at all time points in RUES2 cells but progressively increased in H9 cells over time, reaching a peak at DIV10 (Fig. 3C; Fig. S4A). This finding is in line with the propensity of H9 cells to differentiate into MSNs. RUES2 cells also exhibit strong and unique upregulation of BMP4 and BMP5 ligands compared to H9 and KOLF2 cells, possibly contributing to acquisition of an MGE interneuron identity (Mukhopadhyay et al., 2009) (Fig. 3D; Fig. S4A).

Taken together, these data indicate that H9 and RUES2 human cell lines exposed to the same striatal differentiation protocol acquire different cell identities, possibly due to the activation of different signaling pathways in response to the applied morphogens (Fig. 3E).

3.4. Aberrant telencephalic and MGE cell fate acquisition in isogenic RUES2 carrying different pathological CAG lengths

Several reports have demonstrated that muHTT affects the differentiation and cell fate specification of the human PSC-derived neurons preferentially affected in HD (i.e., the striatal MSNs originating in the LGE and cortical neurons), (Conforti et al., 2018; HD iPSC Consortium 2012, 2017; Ooi et al., 2019; Ring et al., 2015; Ruzo et al., 2018; Smith-Geater et al., 2020; Xu et al., 2017; Ruzo et al., 2018; Mehta et al., 2018). By exploiting the MGE differentiation bias of RUES2, we tested whether muHTT has a similar detrimental effect on this lineage. For these studies, we employed the isogenic HD RUES2 lines with 50 and 58

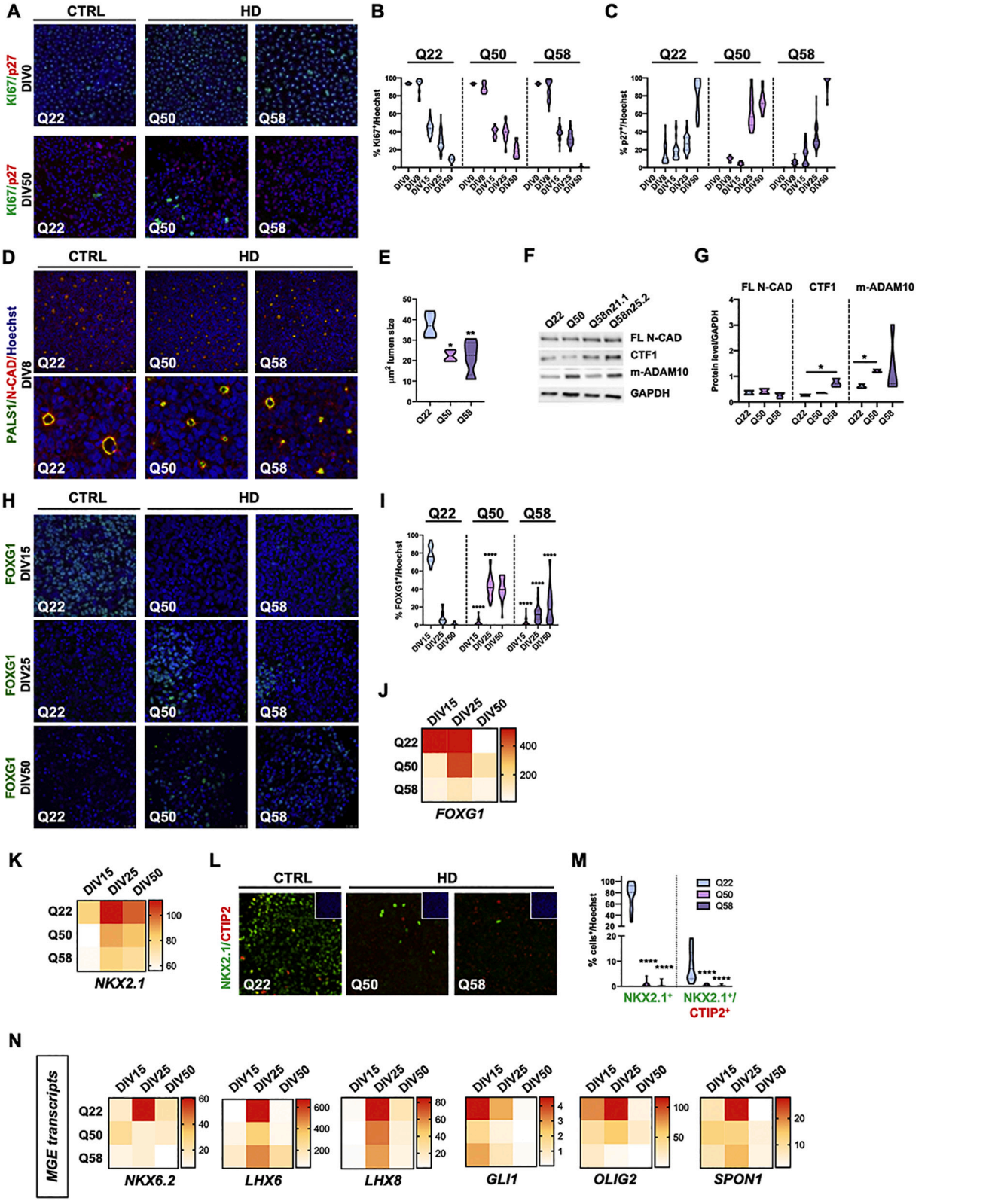

(caption on next page)

Fig. 4. muHTT interferes with telencephalic and MGE cell fate acquisition in HD RUES2 lines.
(A) Immunocytochemistry of Ki67 and p27 at DIV0 and DIV50 of differentiation of the RUES2 control Q22, HD Q50, and HD Q58 lines. Confocal images, 40×. Scale bar, 50 μm.
(B–C) Counts of Ki67$^+$ and p27$^+$ cells for the Q22, Q50, and Q58 RUES2 lines by CellProfiler software (Version 2.1.1). N = 3 biological replicates. Data are presented as mean ± SEM.
(D) Immunocytochemistry of neural rosette formation by N-CAD$^+$/PALS1$^+$ at DIV8 for the RUES2 control Q22, HD Q50, and HD Q58 lines. Confocal images, 40×. Scale bar, 50 μm (crops of N-CAD$^+$/PALS1$^+$ of the same images).
(E) Counts of rosette lumen sizes by CellProfiler software (Version 2.1.1). N = 3 biological replicates. *p < 0.05, **p < 0.01, one-way ANOVA with Tukey's post-hoc test.
(F) Western blot analysis of the full-length N-cadherin (FL N-CAD), CTF1 fragment, and metalloprotease ADAM10 (mADAM10) at DIV8 of differentiation for the RUES2 control Q22, HD Q50, and HD Q58 lines. The FL N-CAD, CTF1, and mADAM10 protein levels in each line were normalized to GAPDH. N = 3 biological replicates.
(G) Violin plot representing the densitometric analysis performed on western blot results from three biological differentiation experiments. *p < 0.05, one-way ANOVA with Tukey's post-hoc test comparing each group condition.
(H) Immunocytochemistry of FOXG1 at DIV15, DIV25, and DIV50 of differentiation for the RUES2 control Q22, HD Q50, and HD Q58 lines. Confocal images, 40×. Scale bar, 50 μm.
(I) FOXG1$^+$ cell counts for the control Q22, HD Q50, and HD Q58 RUES2 lines by CellProfiler software (Version 2.1.1). N = 3 biological replicates. Q50 vs. Q22 and Q58 vs. Q22, ****p < 0.0001, one-way ANOVA with Tukey's post-hoc test.
(J) Heat map showing the expression levels in high-content qPCR analysis (Biomark) of *FOXG1* at DIV15, DIV25, and DIV50 of differentiation for the RUES2 control Q22, HD Q50, and HD Q58 lines.
(K) Heat map showing the expression levels in high-content qPCR analysis (Biomark) of the MGE marker *NKX2.1* at DIV15, DIV25, and DIV50 for the RUES2 control Q22, HD Q50, and HD Q58 lines. N = 3 biological replicates.
(L) Immunocytochemistry of NKX2.1 and CTIP2 at DIV30 for the RUES2 control Q22, HD Q50, and HD Q58 lines. Confocal images, 40×, zoom = 1.7. Scale bar, 50 μm. Top right, Hoechst inset.
(M) Counts of NKX2.1$^+$ and NKX2.1$^+$/CTIP2$^+$ for the control Q22, HD Q50, and HD Q58 RUES2 lines by CellProfiler software (Version 2.1.1). N = 3 biological replicates. ****p < 0.0001, one-way ANOVA.
(N) Heat map showing the expression levels in high-content qPCR analysis (Biomark) of the MGE markers *NKX6,2, LHX6, LHX8, GLI1, OLIG2,* and *SPON1* at DIV15, DIV25, and DIV50 for the RUES2 control Q22, HD Q50, and HD Q58 lines. N = 3 biological replicates.

glutamines and the edited control line carrying Q22 (Fig. S1B) (Ruzo et al., 2018). Normal karyotypes (Fig. S1C) and pluripotency markers were found in all lines (Figs. S5A-M). RUES2 control Q22, HD Q50, and HD Q58 had no significant differences in the number of Ki67$^+$ and p27$^+$ cells from DIV15 to DIV50 (Fig. 4A), suggesting that muHTT does not affect cell cycle exit or neuronal maturation in these cells (Fig. 4B, C), as indicated by phase contrast images (Fig. S5N), immunocytochemistry for TUBB3 and MAP2, and gene transcription analysis for TUBB3, MAP2, and DCX mRNAs (Fig. S5O-R).

Neural rosettes are a stereotypical cell organization of an acquired neuronal phenotype, mimicking the end of neuroectodermal induction. Previous studies have shown that HD-hiPSCs have a smaller lumen size at DIV15 of striatal differentiation (Conforti et al., 2018), whereas HD-RUES2 lines exposed to a default neural induction protocol generate typical neural rosettes with no significant difference (Ruzo et al., 2018). The same HD cellular system exhibits a gradual reduction in lumen size when differentiated into ectodermal neuruloids (Haremaki et al., 2019). Using PALS1 and NCAD markers for rosette lumen identification at DIV8 of *in vitro* differentiation, we confirmed that both the Q50 and Q58 HD RUES2 lines have a significant reduction in rosette lumen area (RUES2 Q22: 37.31 μm^2 ± 5.34; RUES2 Q50: 22.36 μm^2 ± 2.66; RUES2 Q58: 21.6 μm^2 ± 7.61; Fig. 4D, E). Western blot analysis for NCAD confirmed an increase in CTF1 cleavage fragment in HD Q58 cells (two clones; Fig. 4F, G), without changes in NESTIN and NCAD mRNA levels (Fig. S5S, T), which is indicative of an altered capacity of the HD RUES2 cells for cell adhesion and rosette formation.

Next, we monitored the effects of muHTT on ventral telencephalic specification by measuring the acquisition of markers related to a ventral identity. The control Q22 line presented the expected expression profile for FOXG1, with 80 ± 9% of cells immunoreactive at DIV15 and decreasing with time as expected (Fig. 4H, I). In contrast, significantly fewer FOXG1$^+$ cells were found in both HD lines at the same time point (3% ± 2.3 and 4% ± 3 in Q50 and Q58, respectively), with the positive cell peak shifting several weeks for the Q50 line, which remained much lower than in control cells, whereas HD Q58 cultures had a maximum of 11 ± 9% and 15 ± 13% FOXG1$^+$ cells at DIV25 and DIV50, respectively (Fig. 4H, I). Gene expression analysis performed from DIV15 to DIV50 confirmed a reduction in FOXG1 mRNA in the RUES HD line versus control (Fig. 4 J) and, consequently, a further reduction in the percentage of GSX2$^+$/ASCL1$^+$ ventral progenitors at DIV25 and CTIP2$^+$ at DIV50 (Fig. S6A-D). These data indicate that muHTT also causes a delay in telencephalic fate acquisition in ventralized RUES2 cells.

After observing that the RUES2 line acquired a more ventral fate than the H9 line, we explored the impact of muHTT on MGE transcripts. Although NKX2.1 has been linked to MGE development, it is co-expressed with ISL1 and CTIP2, suggesting that NKX2.1 plays a role in LGE formation (Elias et al., 2008; Onorati et al., 2014). QPCR analyses showed up-regulation of NKX2.1 mRNA in control Q22 cells starting from DIV15 (Fig. 4 K), whereas the HD RUES lines exhibited delayed expression of this transcript, which remained at levels below control for the entire period of differentiation (Fig. 4 K). Similarly, in control Q22 cultures, NKX2.1$^+$ cells increased over time, reaching 80% at DIV50; in both HD lines, we observed a complete loss of this cell population (Fig. 4 L, M). In the RUES2 Q22 line, we found that only 10% of NKX2.1$^+$ cells co-expressed CTIP2, confirming that this hESC line has greater ventral identity under these experimental conditions (Fig. 4 L, M). No NKX2.1$^+$/CTIP2$^+$ double-positive progenitors were found in the RUES2 HD lines. Gene transcription analysis performed on a larger set of MGE markers, including NKX6.2, LHX6, LHX8, GLI1, OLIG2, SPON1, and GSX1 corroborated these results, suggesting a negative effect of muHTT in MGE fate determination (Fig. 4 N).

3.5. Isogenic RUES2 lines recapitulate HD phenotypes

To further assess the ability of RUES2 lines to recapitulate known HD phenotypes, we performed a high-content qPCR analysis for transcripts involved in neurodevelopment that are known to be affected by muHTT. REST/NRSF is part of a repressor complex that acts as a central negative regulator of neuronal gene transcription (Ballas and Mandel, 2005; Chong et al., 1995; Schoenherr and Anderson, 1995). Excessive nuclear access of REST/NRSF in HD cells and tissues has been found to reduce the transcription of several neuronal genes, including BDNF (Zuccato et al., 2011; Zuccato and Cattaneo, 2009). Consistently, our qPCR of *BDNF* in neurons derived from RUES2 HD and control lines showed significant downregulation in both HD Q50 and HD Q58 cells

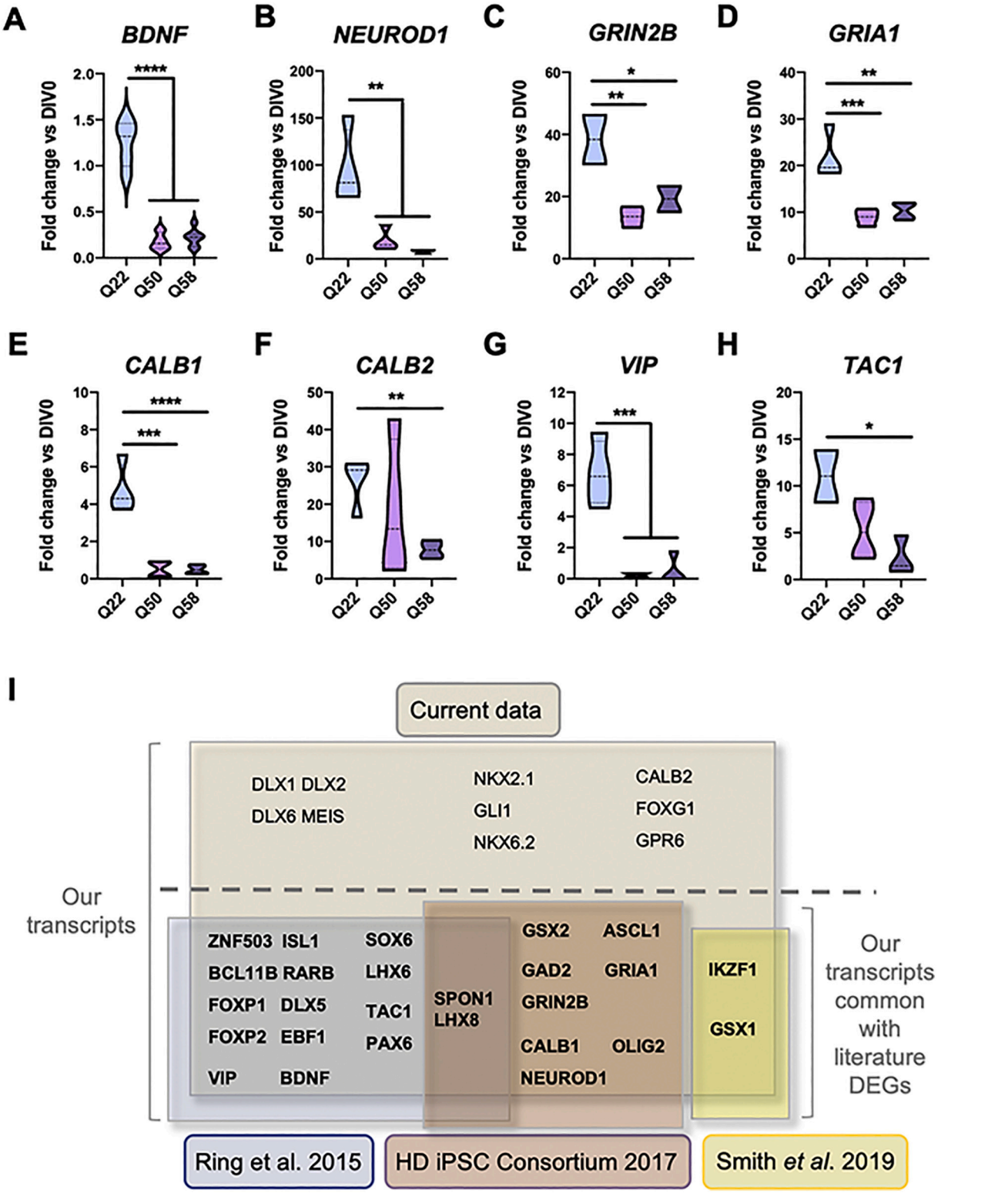

Fig. 5. Isogenic RUES2 lines recapitulate the HD phenotype.
(A-H) QPCR of transcripts known to be altered in mouse and cellular HD models at DIV30 for the RUES2 control Q22, HD Q50, and HD Q58 lines (total mRNA level normalized to 18 s housekeeping transcript). N = 3 biological replicates. *BDNF:* Q50 vs. Q22, ****p < 0.0001; Q58 vs. Q22, ****p < 0.0001. *NEUROD1:* Q50 vs. Q22, **p < 0.01; Q58 vs. Q22, **p < 0.01. *GRIN2B:* Q50 vs. Q22, **p < 0.01; Q58 vs. Q22, *p < 0.05. *GRIA1:* Q50 vs. Q22, ***p < 0.001. Q58 vs. Q22, **p < 0.01. *CALB1:* Q50 vs. Q22, ***p < 0.001; Q58 vs. Q22, ****p < 0.0001. *CALB2:* Q58 vs. Q22, **p < 0.001. *VIP:* Q50 vs. Q22, ***p < 0.001; Q58 vs. Q22, ***p < 0.001. *TAC1:* Q58 vs. Q22, *p < 0.05, one-way ANOVA with Tukey's post-hoc test.
(I) Schematic diagram showing our differential transcripts (current data). Transcripts we found to be in common with differentially expressed genes (DEGs) from studies comparing control and HD lines are showed in bold.

compared to control Q22 cells (Fig. 5A). BDNF levels were also reduced in HD-iPS lines upon exposure to the same differentiation protocol and to cortical differentiation (Shi et al., 2012) (Fig. S7A).

NEUROD1 is controlled by REST/NRSF and has been implicated in aberrant developmental and adult neurogenesis in R6/2 mice and HD iPSC-derived neurons (HD iPSC Consortium, 2017). Both HD RUES2 Q50 and Q58 lines exhibit a significant reduction in NEUROD1 mRNA at DIV30 of differentiation (Fig. 5B). Developmental genes *GRIN2B* and *GRIA1* (Endele et al., 2010) were also reduced in Q50 and Q58 RUES2-derived neurons (Fig. 5C, D), as were CALB1 and CALB2, two calcium binding proteins expressed early in development (Al-Jaberi et al., 2015) (Fig. 5E, F). Other transcripts known to be altered in HD and linked to central nervous system development were also investigated. The neuropeptide vasoactive intestinal polypeptide (VIP), which is highly expressed in the central nervous system, is reduced in R6/2 mice (Fahrenkrug et al., 2007) and significantly reduced in our HD RUES2-derived neurons (Fig. 5G). Similarly, the striatal transcript TAC1, the expression of which is sustained by BDNF (Xie et al., 2010), was reduced in the RUES2 HD lines (Fig. 5H).

To address whether the differentially expressed genes (DEGs) were shared by other HD *in vitro* systems, we interrogated available RNAseq datasets from Ring et al. (2015), the HD iPSC Consortium (2017), and Smith-Geater et al. (2020) and found that several LGE genes were common to all studies, including certain MGE transcripts. In particular, SPON1 and LHX8 were differentially expressed in our analysis and in the Ring et al. (2015) and the HD iPSC Consortium datasets (Fig. 5I). This comparison revealed that common genes were similarly affected in diverse HD hPSC lines exposed to different striatal differentiation protocols, showing the ability of the RUES2 model system to recapitulate mouse and human HD phenotypes.

3.6. *De novo motif discovery analysis identifies SP1 as a potential common regulator in HD neural differentiation*

As muHTT-driven dysregulation appears to affect multiple neuronal lineages (Fig. 6A) (Conforti et al., 2018; HD iPSC Consortium, 2012, 2017; Ooi et al., 2019; Ring et al., 2015; Ruzo et al., 2018; Smith-Geater et al., 2020; Xu et al., 2017), we attempted to identify common regulators of muHTT toxicity by comparing HD-related DEGs using transcriptional data from the above-mentioned studies (Ring et al., 2015; HD iPSC Consortium, 2017; Smith-Geater et al., 2020).

First, we looked at whether the upstream regions of the DEGs characterizing HD hPSCs undergoing LGE, MGE, and cortical differentiation *in vitro* were enriched for specific motifs of TFs that may be affected by muHTT. We employed two different *de novo* motif discovery tools to identify the common TF binding motifs: Multiple EM For Motif Elicitation (MEME) and Oligo Analysis (RSAT) (Bailey et al., 2009; Nguyen et al., 2018) (Fig. S8A). Next, we compared the sequence of the identified motifs with a series of databases of known TF binding sites using STAMP (Mahony and Benos, 2007), a toolkit for comparing DNA motifs that relies on the JASPAR (Bryne et al., 2008) and TRANSFAC (Matys et al., 2003) databases (Fig. S78A; SI1, SI2, SI3). Only the TFs represented by both motif discovery tools were considered further (Fig. S8B). As shown in Fig. 6B, the most significant LGE-specific TFs included SP1 and LHX3, followed by CREB1, KLF4, and SPI1.

The TFs SP1 and RREB1 had the highest scores in the same analysis for MGE and cortex (Fig. 6B). Specifically, the RREB1 protein recognizes and binds RAS-responsive elements (RREs) in gene regulatory regions, and potentiates the transcriptional activity of NEUROD1 (Ray et al., 2014). Lastly, the analysis identified RAP1 as MGE-specific; the protein regulates several signaling pathways affecting cell proliferation and adhesion, as well as the neuronal response to dopamine (Zhang et al., 2018) (Fig. 6B).

Notably, using both databases, STAMP analysis revealed SP1, SPI1, and KLF4 as common putative TFs potentially regulating the DEGs identified in the LGE, MGE, and cortex (Fig. 6B). In particular, SP1 reached the highest significant score in the analysis of signaling pathways (Fig. S9A, B; Table S1 and SI4).

Next, in an attempt to identify gene networks potentially affected by the aberrant SP1-HTT interaction, the DEGs identified by the in silico analyses and the predicted TFs were submitted to the protein interaction database Pathway Commons (http://www.pathwaycommons.org). Using Cytoscape for graphical representation, we found that the DEGs and TFs were connected in an intricate network by both direct binding and transcriptional regulation. The analysis highlighted the direct interaction between SP1 and HTT in all areas analyzed (Fig. 6C-E; Table S1).

4. Discussion

As hPSCs can efficiently differentiate into functional neurons through processes that recapitulate in vivo development, the use of small molecules and morphogens to drive hPSCs towards the acquisition of a coordinated antero/posterior or ventral/dorsal fate allows the generation of specific neurons essential for modeling neurodegenerative diseases. Patterning during *in vitro* neural differentiation is regulated by retinoic acid and the FGF and BMP families, with a prominent role of SHH signaling in ventralization (Germain et al., 2013; Li et al., 2009; Liu et al., 2013; Maroof et al., 2013; Nicholas et al., 2013) and WNT signaling in both dorsalization and caudalization (Elkabetz et al., 2008; Kirkeby et al., 2012; Li et al., 2009).

Here, the RUES2 line presented a different expression profile in SHH, WNT, RA, and BMP signaling compared to the H9 and KOLF2 lines. The hyperactivation of SHH signaling, together with the upregulation of BMP4 and BMP5 ligands and the complete loss of RARβ expression, suggests that the RUES2 lines are more ventralized than the H9 and KOLF2 lines. In line with this data, Strano et al. (2020) demonstrated that the patterning variation of different hESCs is associated with differences in SHH and WNT signaling dynamics and that early differences in regional gene expression were predictive of late-stage fate acquisition (Strano et al., 2020). Earlier studies have reported marked differences in differentiation propensities among different human embryonic stem cell lines (Osafune et al., 2008), further pointing to the relevance of deriving multiple lines for lineage-specific differentiation (Wu et al., 2007; Hu et al., 2010).

In our experiments, control RUES2 cells exposed to the striatal differentiation protocol exhibited impairment in the acquisition of an MSN striatal fate, compared to H9 and KOLF2 cells. In particular, the RUES2 line failed to express the MSN regulator DARPP32 while preferentially upregulating MGE-enriched transcripts. This is suggested by simultaneous expression of NKX2.1, LHX6 and LHX8 and other transcripts qualifying MGE GABAergic interneurons, such as GAD67. Leveraging the RUES2 MGE-biased differentiation potential, we show that muHTT interferes with MGE cell fate acquisition, as already demonstrated for LGE (Ring et al., 2015; HD iPSC Consortium, 2017; Xu et al., 2017; Conforti et al., 2018; Smith-Geater et al., 2020) and cortical neurons (Conforti et al., 2018; Ruzo et al., 2018; Mehta et al., 2018; Ooi et al., 2019). MGE GABAergic interneurons are essential for neural circuit function (Tremblay et al., 2016), and their loss or dysfunction is implicated in several human psychiatric disorders, including autism, schizophrenia, and epilepsy (Marín, 2012). Our data suggest that muHTT negatively influences MGE-interneuron differentiation, opening up the possibility that MGE derivatives may make a greater contribution to HD than previously thought.

Our observations also point to the presence of common muHTT-related interactors whose activity is shared by the different lineage-specific signaling pathways that interact during neurogenesis. SP1 is a TF found in all mammalian cell types that plays a central role in several human diseases, including HD. Several lines of evidence link SP1 to HTT, demonstrating their direct interaction in transgenic HD mouse brain, striatal HD cells, and human HD brain (Dunah et al., 2002). In particular, the N-terminal portion of muHTT interacts more strongly

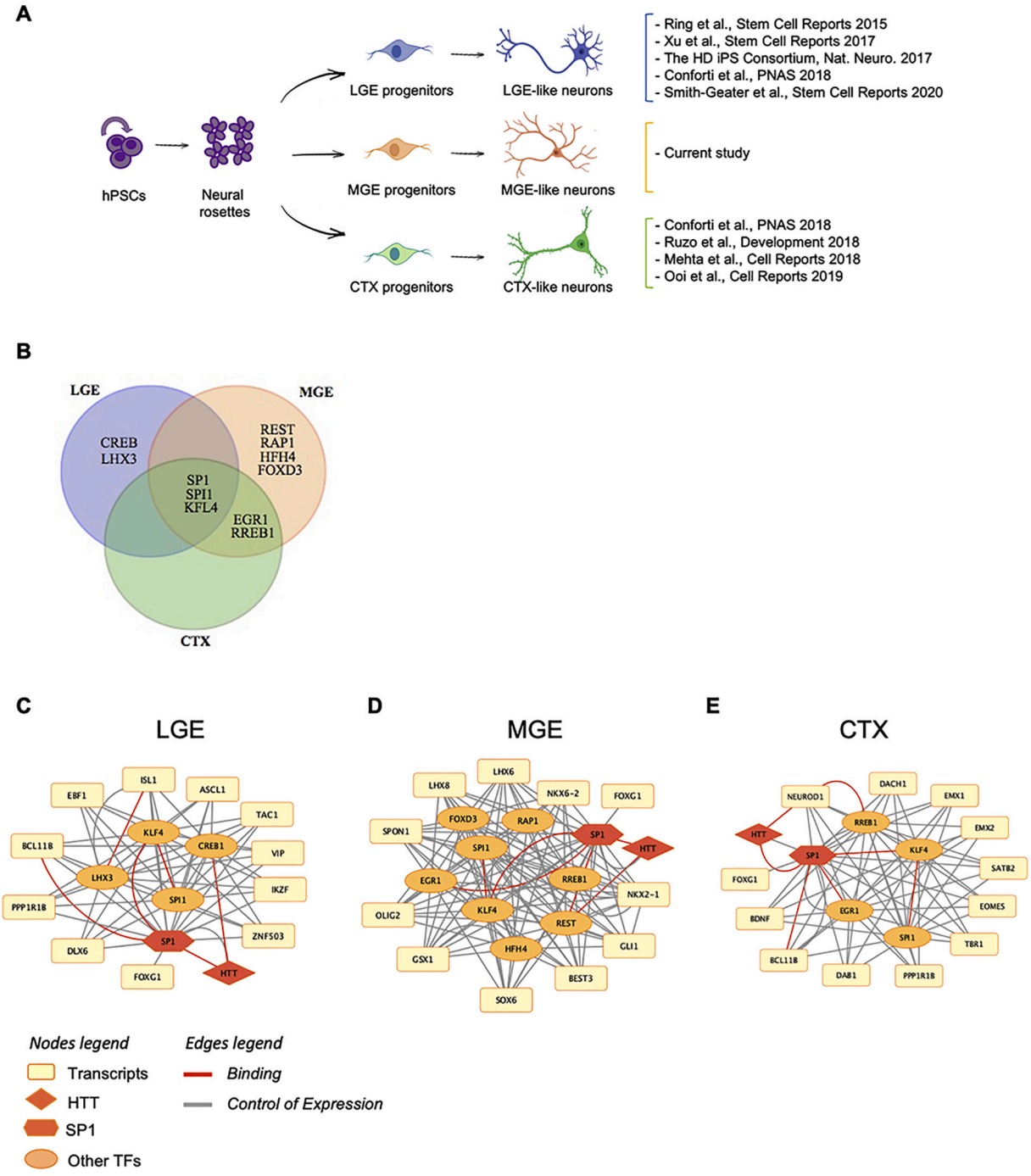

Fig. 6. *De novo* motif discovery analysis identified Sp1 as a potential common regulator in neural differentiation.
(A) Schematic representation of the papers reported in the literature differentiating iPSCs and hESCs in different neuronal lineages (LGE, MGE, and CTX). The presence of muHTT may impact the ability to differentiate into multiple neuronal types, and this constitutes the rationale for the *de novo* motif discovery analysis.
(B) Venn diagram of the unique and shared LGE, MGE, and cortical predictive transcription factors (TFs) identified by *de novo* motif discovery analysis.
(C-E) Cytoscape networks for LGE, MGE, and CTX, representing the predicted interactions obtained by *de novo* motif discovery analysis enriched with the molecular and genetic interactions and gene regulation networks generated by Pathway Commons (https://apps.pathwaycommons.org/interactions). The TFs submitted to the *de novo* motif discovery analysis specific for each brain area are depicted in yellow, and in orange are the common regulators. Sp1 is highlighted in red because it was the most represented and relative to HTT. The binding interactions are reported in red and controlled expression in grey.

with SP1 than non-pathologic HTT, resulting in cytoplasmic retention of the TF in HD and reduced nuclear SP1, leading to reduced occupancy of the promoters of SP1-responsive genes, such as DRD2 (Chen-Plotkin et al., 2006; Dunah et al., 2002), REST (Ravache et al., 2010), and HTT itself (Wang et al., 2012).

A second transcriptional regulator that potentially plays a role in modulating HD-related gene signaling is SPI1 or PU.1, which encodes a protein involved in the regulation of several cellular processes, including cell differentiation, cell growth, apoptosis, DNA damage response, and chromatin remodeling. In particular, SPI1 controls a variety of myeloid genes that are important for brain inflammation and neuroimmunology. Crotti et al. (2014) found that the presence of muHTT in microglia promotes cell-autonomous pro-inflammatory transcriptional activation by increasing the expression and activation of the

transcription of SPI1.

A third TF that emerged from the analysis is Krueppel-like factor 4 (KLF4), an important regulator of early embryonic development, as it contributes to maintaining self-renewal and preventing hESC differentiation. KLF4 is also a powerful negative regulator of the expression of multiple smooth muscle cell (SMC) genes through its activation by SP1 (Deaton et al., 2009; Zhang et al., 2012).

The data from our *in-silico* analysis showed that, in the LGE context, LHX3 is a potential common mediator of signaling. Interestingly, SP1 controls and interacts with LHX3 (Yaden et al., 2006). This gene encodes a protein that, by acting as a transcriptional activator, regulates pituitary development and motor neuron specification through the interaction with ISL1 (Erb et al., 2017; Lee et al., 2012a, 2012b, 2012c; Seo et al., 2015; Thaler et al., 2002).

We also found LGE-specific alterations in the transcription of the cAMP response element-binding protein (CREB), which has already been associated with HD as a possible contributor to neuronal cell death and dysfunction (Wyttenbach, 2001). The CREB pathway involves the activity of TAFII130, a coactivator found in polyQ aggregates that, when overexpressed, can rescue HD reduction in CREB-dependent transcription (Shimohata et al., 2000). Dunah et al. (2002) reported that the expanded polyQ of muHTT impairs the soluble association of TAFII130 with SP1 through direct interference in SP1 binding to the DNA.

The discovery of SP1 as the most common predictive TF of the *de novo* motif discovery analysis is supported by several lines of evidence in the literature, highlighting SP1 as a possible common player in the abnormal neuronal gene transcription profiles identified thus far in all studies that have employed HD-hPSC lines, suggesting SP1 as a potential detrimental co-partner of muHTT during neuronal differentiation.

Overall, this work highlights the different propensity of various hPSCs to acquire a specific cell fate when exposed to the striatal differentiation protocol. The RUES2 line exhibited MGE-biased neuronal differentiation that is compromised by muHTT. *In silico de novo* motif discovery analysis identified the TF SP1 as a putative common regulator of the DEGs specific for different cerebral areas. Therefore, we hypothesize that, in the presence of muHTT, the broad transcriptional activity of SP1 is compromised and this interferes with cell fate commitment.

Acknowledgments

This work was funded by CHDI Foundation, Inc. New York, (JSC A11103) a nonprofit biomedical research organization exclusively dedicated to developing therapeutics that will substantially improve the lives of HD-affected individuals and, partially, by the European Union Model PolyQ research project within the framework of the Joint Call (JPND), with funding from the corresponding JPND National Funding Agencies. We thank Ali H. Brivanlou for the RUES2 cell lines, Bill Skarnes for the KOLF2 cell line and Alessio Buscaglia for the support in implementing the *in silico* analysis.

Author contributions

P.C., D.B., and E.C. designed the research; P.C., S.B., and A.L. performed the *in vitro* studies; S.B. performed the bioinformatics *in silico* analysis with contributions from R.R.; I.C. helped with WB experiments.; M.G. contributed to cell line maintenance and characterization; C.C. and V.D.B. contributed to the analyses of the high-content qPCR data; R.I. quantified the lumen area; and P.C., D.B., S.B., and E.C. wrote the paper.

Credit Authors Statement

P.C., D.B., and E.C. designed the research.

P.C., S.B., and A.L. performed the *in vitro* studies.

S.B. performed the bioinformatics in silico analysis with contributions from R.R.

I.C. helped with WB experiments.

M.G. contributed to cell line maintenance and characterization.

C.C. and V.D.B. contributed to the analyses of the high-content qPCR data.

R.I. quantified the lumen area.

P.C., D.B., S.B., and E.C. wrote the paper.

Declaration of Competing Interest

The authors declare no competing interests.

Appendix A. Supplementary data

Supplementary data to this article can be found online at https://doi.org/10.1016/j.nbd.2020.105140.

References

Al-Jaberi, N., Lindsay, S., Sarma, S., Bayatti, N., Clowry, G.J., 2015. The early fetal development of human neocortical GABAergic interneurons. Cereb. Cortex. https://doi.org/10.1093/cercor/bht254.

Ballas, N., & Mandel, G. (2005). The many faces of REST oversee epigenetic programming of neuronal genes. In Current Opinion in Neurobiology. https://doi.org/10.1016/j.conb.2005.08.015.

Bailey, T.L., Boden, M., Buske, F.A., Frith, M., Grant, C.E., Clementi, L., Ren, J., Li, W.W., Noble, W.S., 2009. MEME suite: tools for motif discovery and searching. Nucleic Acids Res. https://doi.org/10.1093/nar/gkp335.

Barnat, M., Capizzi, M., Aparicio, E., Boluda, S., Wennagel, D., Kacher, R., Kassem, R., Lenoir, S., Agasse, F., Bra, B.Y., Liu, J.P., Ighil, J., Tessier, A., Zeitli, S.O., Duyckaerts, C., Dommergues, M., Durr, A., Humbert, S., 2020. Huntington's disease alters human neurodevelopment. Science. https://doi.org/10.1126/science.aax3338.

Besusso, D., Schellino, R., Boido, M., Belloli, S., Parolisi, R., Conforti, P., Faedo, A., Cernigoj, M., Campus, I., Laporta, A., Bocchi, V.D., Murtaj, V., Parmar, M., Spaiardi, P., Talpo, F., Maniezzi, C., Toselli, M.G., Biella, G., Moresco, R.M., ... Cattaneo, E., 2020. Stem cell-derived human striatal progenitors innervate striatal targets and alleviate sensorimotor deficit in a rat model of Huntington disease. Stem Cell Rep. https://doi.org/10.1016/j.stemcr.2020.03.018.

Bryne, J.C., Valen, E., Tang, M.H.E., Marstrand, T., Winther, O., Da piedade, I., Krogh, A., Lenhard, B., Sandelin, A., 2008. JASPAR, the open access database of transcription factor-binding profiles: New content and tools in the 2008 update. Nucleic Acids Res. https://doi.org/10.1093/nar/gkm955.

Chambers, S.M., Fasano, C.A., Papapetrou, E.P., Tomishima, M., Sadelain, M., Studer, L., 2009. Highly efficient neural conversion of human ES and iPS cells by dual inhibition of SMAD signaling. Nature Biotechnology. https://doi.org/10.1038/nbt.1529.

Chatzi, C., Brade, T., Duester, G., 2011. Retinoic acid functions as a key gabaergic differentiation signal in the basal ganglia. PLoS Biol. https://doi.org/10.1371/journal.pbio.1000609.

Chen-Plotkin, A.S., Sadri-Vakili, G., Yohrling, G.J., Braveman, M.W., Benn, C.L., Glajch, K.E., DiRocco, D.P., Farrell, L.A., Krainc, D., Gines, S., MacDonald, M.E., Cha, J.H.J., 2006. Decreased association of the transcription factor Sp1 with genes down-regulated in Huntington's disease. Neurobiol. Dis. https://doi.org/10.1016/j.nbd.2005.11.001.

Chi, L., Fan, B., Zhang, K., Du, Y., Liu, Z., Fang, Y., Chen, Z., Ren, X., Xu, X., Jiang, C., Li, S., Ma, L., Gao, L., Liu, L., Zhang, X., 2016. Targeted differentiation of regional ventral Neuroprogenitors and related neuronal subtypes from human pluripotent stem cells. Stem Cell Rep. https://doi.org/10.1016/j.stemcr.2016.09.003.

Chong, J.A., Tapia-Ramirez, J., Kim, S., Toledo-Aral, J.J., Zheng, Y., Boutros, M.C., Altshuller, Y.M., Frohman, M.A., Kraner, S.D., Mandel, G., 1995. REST: A mammalian silencer protein that restricts sodium channel gene expression to neurons. Cell. https://doi.org/10.1016/0092-8674(95)90298-8.

Conforti, P., Besusso, D., Bocchi, V.D., Faedo, A., Cesana, E., Rossetti, G., Ranzani, V., Svendsen, C.N., Thompson, L.M., Toselli, M., Biella, G., Pagani, M., Cattaneo, E., 2018. Faulty neuronal determination and cell polarization are reverted by modulating HD early phenotypes. Proc. Natl. Acad. Sci. U. S. A. https://doi.org/10.1073/pnas.1715865115.

Crotti, A., Benner, C., Kerman, B.E., Gosselin, D., Lagier-Tourenne, C., Zuccato, C., Cattaneo, E., Gage, F.H., Cleveland, D.W., Glass, C.K., 2014. Mutant Huntingtin promotes autonomous microglia activation via myeloid lineage-determining factors. Nat. Neurosci. https://doi.org/10.1038/nn.3668.

Deaton, R.A., Gan, Q., Owens, G.K., 2009. Spl-dependent activation of KLF4 is required for PDGF-BB-induced phenotypic modulation of smooth muscle. Am. J. Physiol. Heart Circ. Physiol. https://doi.org/10.1152/ajpheart.01230.2008.

Delli Carri, A., Onorati, M., Castiglioni, V., Faedo, A., Camnasio, S., Toselli, M., Biella, G., Cattaneo, E., 2013. Human pluripotent stem cell differentiation into authentic striatal projection neurons. Stem Cell Rev. Rep. https://doi.org/10.1007/s12015-013-9441-8.

Dunah, A.W., Jeong, H., Griffin, A., Kim, Y.M., Standaert, D.G., Hersch, S.M., Mouradian, M.M., Young, A.B., Tanese, N., Krainc, D., 2002. Sp1 and TAFII130 transcriptional activity disrupted in early Huntington's disease. Science. https://doi.org/10.1126/science.1072613.

Elias, L.A.B., Potter, G.B., Kriegstein, A.R., 2008. A time and a place for Nkx2-1 in interneuron specification and migration. Neuron. https://doi.org/10.1016/j.neuron.2008.08.017.

Elkabetz, Y., Panagiotakos, G., Al Shamy, G., Socci, N.D., Tabar, V., Studer, L., 2008. Human ES cell-derived neural rosettes reveal a functionally distinct early neural stem cell stage. Genes Dev. https://doi.org/10.1101/gad.1616208.

Endele, S., Rosenberger, G., Geider, K., Popp, B., Tamer, C., Stefanova, I., Milh, M., Kortüm, F., Fritsch, A., Pientka, F.K., Hellenbroich, Y., Kalscheuer, V.M., Kohlhase, J., Moog, U., Rappold, G., Rauch, A., Ropers, H.H., Von Spiczak, S., Tönnies, H., ... Kutsche, K., 2010. Mutations in GRIN2A and GRIN2B encoding regulatory subunits of NMDA receptors cause variable neurodevelopmental phenotypes. Nat. Genet. https://doi.org/10.1038/ng.677.

Erb, M., Lee, B., Seo, S.Y., Lee, J.W., Lee, S., Lee, S.K., 2017. The isl1-lhx3 complex promotes motor neuron specification by activating transcriptional pathways that enhance its own expression and formation. ENeuro. https://doi.org/10.1523/ENEURO.0349-16.2017.

Fahrenkrug, J., Popovic, N., Georg, B., Brundin, P., Hannibal, J., 2007. Decreased VIP and VPAC2 receptor expression in the biological clock of the R6/2 Huntington's disease mouse. J. Mol. Neurosci. https://doi.org/10.1385/jmn/31:02:139.

Farshim, P.P., Bates, G.P., 2018. Mouse models of Huntington's disease. Methods Mol. Biol. https://doi.org/10.1007/978-1-4939-7825-0_6.

Fasano, C.A., Chambers, S.M., Lee, G., Tomishima, M.J., Studer, L., 2010. Efficient derivation of functional floor plate tissue from human embryonic stem cells. Cell Stem Cell. https://doi.org/10.1016/j.stem.2010.03.001.

Germain, N.D., Banda, E.C., Becker, S., Naegele, J.R., Grabel, L.B., 2013. Derivation and isolation of NKX2.1-positive basal forebrain progenitors from human embryonic stem cells. Stem Cells Dev. https://doi.org/10.1089/scd.2012.0264.

Godin, J.D., Colombo, K., Molina-Calavita, M., Keryer, G., Zala, D., Charrin, B.E.C., Dietrich, P., Volvert, M.L., Guillemot, F., Dragatsis, I., Bellaiche, Y., Saudou, F., Nguyen, L., Humbert, S., 2010. Huntingtin is required for mitotic spindle orientation and mammalian neurogenesis. Neuron. https://doi.org/10.1016/j.neuron.2010.06.027.

Gusella, J.F., MacDonald, M.E., 2006. Huntington's disease: seeing the pathogenic process through a genetic lens. Trends Biochem. Sci. https://doi.org/10.1016/j.tibs.2006.06.009.

Haremaki, T., Metzger, J.J., Rito, T., Ozair, M.Z., Etoc, F., Brivanlou, A.H., 2019. Self-organizing neuruloids model developmental aspects of Huntington's disease in the ectodermal compartment. Nat. Biotechnol. https://doi.org/10.1038/s41587-019-0237-5.

Hasenpusch-Theil, K., Watson, J.A., Theil, T., 2017. Direct Interactions Between Gli3, Wnt8b and Fgfs Underlie Patterning of the Dorsal Telencephalon. Cereb. Cortex (New York, N.Y. : 1991). https://doi.org/10.1093/cercor/bhv291.

HD iPSC Consortium, Mattis, V.B., Svendsen, S.P., Ebert, A., Svendsen, C.N., King, A.R., Casale, M., Winokur, S.T., Batugedara, G., Vawter, M., Donovan, P.J., Lock, L.F., Thompson, L.M., Zhu, Y., Fossale, E., Atwal, R.S., Gillis, T., Mysore, J., Li, J.H., ... Arjomand, J., 2012. Induced pluripotent stem cells from patients with huntington's disease show CAG repeat expansion associated phenotypes. Cell Stem Cell. https://doi.org/10.1016/j.stem.2012.04.027.

HD iPSC Consortium, Lim, R.G., Salazar, L.L., Wilton, D.K., King, A.R., Stocksdale, J.T., Sharifabad, D., Lau, A.L., Stevens, B., Reidling, J.C., Winokur, S.T., Casale, M.S., Thompson, L.M., Pardo, M., Díaz-Barriga, A.G.G., Straccia, M., Sanders, P., Alberch, J., Canals, J.M., ... Svendsen, C.N., 2017. Developmental alterations in Huntington's disease neural cells and pharmacological rescue in cells and mice. Nat. Neurosci. https://doi.org/10.1038/nn.4532.

Hu, B.-Y., Weick, J.P., Yu, J., Ma, L.-X., Zhang, X.-Q., Thomson, J.A., Zhang, S.-C., 2010. Neural differentiation of human induced pluripotent stem cells follows developmental principles but with variable potency. Proceedings of the National Academy of Sciences of the United States of America. https://doi.org/10.1073/pnas.0910012107.

Kirkeby, A., Grealish, S., Wolf, D.A., Nelander, J., Wood, J., Lundblad, M., Lindvall, O., Parmar, M., 2012. Generation of regionally specified neural progenitors and functional neurons from human embryonic stem cells under defined conditions. Cell Rep. https://doi.org/10.1016/j.celrep.2012.04.009.

Lee, S., Cuvillier, J.M., Lee, B., Shen, R., Lee, J.W., Lee, S.K., 2012a. Fusion protein Isl1-Lhx3 specifies motor neuron fate by inducing motor neuron genes and concomitantly suppressing the interneuron programs. Proc. Natl. Acad. Sci. U. S. A. https://doi.org/10.1073/pnas.1114515109.

Lee, J.K., Mathews, K., Schlaggar, B., Perlmutter, J., Paulsen, J.S., Epping, E., Burmeister, L., Nopoulos, P., 2012b. Measures of growth in children at risk for Huntington disease. Neurology. https://doi.org/10.1212/WNL.0b013e3182648b65.

Lee, J.M., Ramos, E.M., Lee, J.H., Gillis, T., Mysore, J.S., Hayden, M.R., Warby, S.C., Morrison, P., Nance, M., Ross, C.A., Margolis, R.L., Squitieri, F., Orobello, S., Di Donato, S., Gomez-Tortosa, E., Ayuso, C., Suchowersky, O., Trent, R.J.A., McCusker, E., ... Gusella, J.F., 2012c. CAG repeat expansion in Huntington disease determines age at onset in a fully dominant fashion. Neurology. https://doi.org/10.1212/WNL.0b013e318249f683.

Li, X.J., Zhang, X., Johnson, M.A., Wang, Z.B., LaVaute, T., Zhang, S.C., 2009. Coordination of sonic hedgehog and Wnt signaling determines ventral and dorsal telencephalic neuron types from human embryonic stem cells. Development. https://doi.org/10.1242/dev.036624.

Lin, C.H., Tallaksen-Greene, S., Chien, W.M., Cearley, J.A., Jackson, W.S., Crouse, A.B., Ren, S., Li, X.J., Albin, R.L., Detloff, P.J., 2001. Neurological abnormalities in a knock-in mouse model of Huntington's disease. Hum. Mol. Genet. https://doi.org/10.1093/hmg/10.2.137.

Liu, Y., Liu, H., Sauvey, C., Yao, L., Zarnowska, E.D., Zhang, S.C., 2013. Directed differentiation of forebrain GABA interneurons from human pluripotent stem cells. Nat. Protoc. https://doi.org/10.1038/nprot.2013.106.

Lopes, C., Aubert, S., Bourgois-Rocha, F., Barnat, M., Rego, A.C., Déglon, N., Perrier, A.L., Humbert, S., 2016. Dominant-negative effects of adult-onset huntingtin mutations alter the division of human embryonic stem cells-derived neural cells. PLoS One. https://doi.org/10.1371/journal.pone.0148680.

Lucas, J.J., Ortega, Z., 2011. Animal Models for Huntington ' S Disease. (Animal Models for Neurodegenerative Disease).

Ma, L., Wang, Y., Hui, Y., Du, Y., Chen, Z., Feng, H., Zhang, S., Li, N., Song, J., Fang, Y., Xu, X., Shi, L., Zhang, B., Cheng, J., Zhou, S., Liu, L., Zhang, X., 2019. WNT/NOTCH pathway is essential for the maintenance and expansion of human MGE progenitors. Stem Cell Rep. 12 (5), 934–949. https://doi.org/10.1016/j.stemcr.2019.04.007.

Mahony, S., Benos, P.V., 2007. STAMP: A web tool for exploring DNA-binding motif similarities. Nucleic Acids Res. https://doi.org/10.1093/nar/gkm272.

Marín, O., 2012. Interneuron dysfunction in psychiatric disorders. Nat. Rev. Neurosci. https://doi.org/10.1038/nrn3155.

Maroof, A.M., Keros, S., Tyson, J.A., Ying, S.W., Ganat, Y.M., Merkle, F.T., Liu, B., Goulburn, A., Stanley, E.G., Elefanty, A.G., Widmer, H.R., Eggan, K., Goldstein, P.A., Anderson, S.A., Studer, L., 2013. Directed differentiation and functional maturation of cortical interneurons from human embryonic stem cells. Cell Stem Cell. https://doi.org/10.1016/j.stem.2013.04.008.

Matys, V., Fricke, E., Geffers, R., Gößling, E., Haubrock, M., Hehl, R., Hornischer, K., Karas, D., Kel, A.E., Kel-Margoulis, O.V., Kloos, D.U., Land, S., Lewicki-Potapov, B., Michael, H., Münch, R., Reuter, I., Rotert, S., Saxel, H., Scheer, M., ... Wingender, E., 2003. TRANSFAC®: transcriptional regulation, from patterns to profiles. Nucleic Acids Res. https://doi.org/10.1093/nar/gkg108.

Mehta, S.R., Tom, C.M., Wang, Y., Bresee, C., Rushton, D., Mathkar, P.P., Tang, J., Mattis, V.B., 2018. Human Huntington's disease iPSC-derived cortical neurons display altered Transcriptomics, morphology, and maturation. Cell Rep. https://doi.org/10.1016/j.celrep.2018.09.076.

Molero, A.E., Gokhan, S., Gonzalez, S., Feig, J.L., Alexandre, L.C., Mehler, M.F., 2009. Impairment of developmental stem cell-mediated striatal neurogenesis and pluripotency genes in a knock-in model of Huntington's disease. Proc. Natl. Acad. Sci. U. S. A. https://doi.org/10.1073/pnas.0912171106.

Molero, A.E., Arteaga-Bracho, E.E., Chen, C.H., Gulinello, M., Winchester, M.L., Pichamoorthy, N., Gokhan, S., Khodakhah, K., Mehler, M.F., 2016. Selective expression of mutant huntingtin during development recapitulates characteristic features of Huntington's disease. Proc. Natl. Acad. Sci. U. S. A. https://doi.org/10.1073/pnas.1603871113.

Mukhopadhyay, A., McGuire, T., Peng, C.Y., Kessler, J.A., 2009. Differential effects of BMP signaling on parvalbumin and somatostatin interneuron differentiation. Development. https://doi.org/10.1242/dev.034439.

Nanetti, L., Contarino, V.E., Castaldo, A., Sarro, L., Bachoud-Levi, A.C., Giavazzi, M., Frittoli, S., Ciammola, A., Rizzo, E., Gellera, C., Bruzzone, M.G., Taroni, F., Grisoli, M., Mariotti, C., 2018. Cortical thickness, stance control, and arithmetic skill: An exploratory study in premanifest Huntington disease. Parkinsonism Relat. Disord. https://doi.org/10.1016/j.parkreldis.2018.02.033.

Nguyen, N.T.T., Contreras-Moreira, B., Castro-Mondragon, J.A., Santana-Garcia, W., Ossio, R., Robles-Espinoza, C.D., Bahin, M., Collombet, S., Vincens, P., Thieffry, D., Van Helden, J., Medina-Rivera, A., Thomas-Chollier, M., 2018. RSAT 2018: regulatory sequence analysis tools 20th anniversary. Nucleic Acids Res. https://doi.org/10.1093/nar/gky317.

Nicholas, C.R., Chen, J., Tang, Y., Southwell, D.G., Chalmers, N., Vogt, D., Arnold, C.M., Chen, Y.J.J., Stanley, E.G., Elefanty, A.G., Sasai, Y., Alvarez-Buylla, A., Rubenstein, J.L.R., Kriegstein, A.R., 2013. Functional maturation of hPSC-derived forebrain interneurons requires an extended timeline and mimics human neural development. Cell Stem Cell. https://doi.org/10.1016/j.stem.2013.04.005.

Nopoulos, P.C., Aylward, E.H., Ross, C.A., Johnson, H.J., Magnotta, V.A., Juhl, A.R., Pierson, R.K., Mills, J., Langbehn, D.R., Paulsen, J.S., 2011. Cerebral cortex structure in prodromal Huntington disease. Neurobiology of Disease. https://doi.org/10.1016/j.nbd.2010.07.014.

Onorati, M., Castiglioni, V., Biasci, D., Cesana, E., Menon, R., Vuono, R., Talpo, F., Laguna Goya, R., Lyons, P.A., Bulfamante, G.P., Muzio, L., Martino, G., Toselli, M., Farina, C., A Barker, R., Biella, G., Cattaneo, E., 2014. Molecular and functional definition of the developing human striatum. Nat. Neurosci. 17 (12), 1804–1815. https://doi.org/10.1038/nn.3860.

Ooi, J., Langley, S.R., Xu, X., Utami, K.H., Sim, B., Huang, Y., Harmston, N.P., Tay, Y.L., Ziaei, A., Zeng, R., Low, D., Aminkeng, F., Sobota, R.M., Ginhoux, F., Petretto, E., Pouladi, M.A., 2019. Unbiased profiling of isogenic Huntington disease hPSC-derived CNS and peripheral cells reveals strong cell-type specificity of CAG length effects. Cell Rep. 26 (9), 2494–2508.e7. https://doi.org/10.1016/j.celrep.2019.02.008.

Osafune, K., Caron, L., Borowiak, M., Martinez, R.J., Fitz-Gerald, C.S., Sato, Y., Cowan, C.A., Chien, K.R., Melton, D.A., 2008. Marked differences in differentiation propensity among human embryonic stem cell lines. Nat. Biotechnol. 26, 313–315. https://doi.org/10.1038/nbt1383.

Osipovitch, M., Asenjo Martinez, A., Mariani, J.N., Cornwell, A., Dhaliwal, S., Zou, L., Chandler-Militello, D., Wang, S., Li, X., Benraiss, S.J., Agate, R., Lampp, A., Benraiss, A., Windrem, M.S., Goldman, S.A., 2019. Human ESC-derived chimeric mouse models of Huntington's disease reveal cell-intrinsic defects in glial progenitor cell differentiation. Cell Stem Cell. https://doi.org/10.1016/j.stem.2018.11.010.

Ramocki, M.B., Zoghbi, H.Y., 2008. Failure of neuronal homeostasis results in common neuropsychiatric phenotypes. Nature. https://doi.org/10.1038/nature07457.

Rataj-Baniowska, et al., 2015. Retinoic acid receptor β controls development of striatonigral projection neurons through FGF-dependent and meis1-dependent mechanisms.

J. Neurosci. 14467–14475. https://doi.org/10.1523/JNEUROSCI.4440-15.2016. Correction.
Ravache, M., Weber, C., Mérienne, K., Trottier, Y., 2010. Transcriptional activation of REST by Sp1 in huntington's disease models. PLoS One. https://doi.org/10.1371/journal.pone.0014311.
Ray, S.K., Li, H.J., Metzger, E., Schule, R., Leiter, A.B., 2014. CtBP and associated LSD1 are required for transcriptional activation by NeuroD1 in gastrointestinal endocrine cells. Mol. Cell. Biol. https://doi.org/10.1128/mcb.01600-13.
Ring, K.L., An, M.C., Zhang, N., O'Brien, R.N., Ramos, E.M., Gao, F., Atwood, R., Bailus, B.J., Melov, S., Mooney, S.D., Coppola, G., Ellerby, L.M., 2015. Genomic analysis reveals disruption of striatal neuronal development and therapeutic targets in human Huntington's disease neural stem cells. Stem Cell Rep. https://doi.org/10.1016/j.stemcr.2015.11.005.
Ruzo, A., Croft, G.F., Metzger, J.J., Galgoczi, S., Gerber, L.J., Pellegrini, C., Wang, H., Fenner, M., Tse, S., Marks, A., Nchako, C., Brivanlou, A.H., 2018. Chromosomal instability during neurogenesis in huntington's disease. Development (Cambridge). https://doi.org/10.1242/dev.156844.
Sampedro, F., Martínez-Horta, S., Perez-Perez, J., Horta-Barba, A., Martin-Lahoz, J., Alonso-Solís, A., Corripio, I., Gomez-Anson, B., Kulisevsky, J., 2019. Widespread increased diffusivity reveals early cortical degeneration in Huntington disease. Am. J. Neuroradiol. https://doi.org/10.3174/ajnr.A6168.
Schoenherr, C.J., Anderson, D.J., 1995. The neuron-restrictive silencer factor (NRSF): a coordinate repressor of multiple neuron-specific genes. Science 267(5202) (5202), 1360–1363. https://doi.org/10.1126/science.7871435.
Seo, S.Y., Lee, B., Lee, S., 2015. Critical roles of the LIM domains of Lhx3 in recruiting Coactivators to the motor neuron-specifying Isl1-Lhx3 complex. Mol. Cell. Biol. https://doi.org/10.1128/mcb.00335-15.
Shi, Y., Kirwan, P., Smith, J., Robinson, H.P.C., Livesey, F.J., 2012. Human cerebral cortex development from pluripotent stem cells to functional excitatory synapses. Nat. Neurosci. https://doi.org/10.1038/nn.3041.
Shimohata, T., Nakajima, T., Yamada, M., Uchida, C., Onodera, O., Naruse, S., Kimura, T., Koide, R., Nozaki, K., Sano, Y., Ishiguro, H., Sakoe, K., Ooshima, T., Sato, A., Ikeuchi, T., Oyake, M., Sato, T., Aoyagi, Y., Hozumi, I., ... Tsuji, S., 2000. Expanded polyglutamine stretches interact with TAF(II)130, interfering with CREB-dependent transcription. Nat. Genet. https://doi.org/10.1038/79139.
Smith, M.A., Brandt, J., Shadmehr, R., 2000. Motor disorder in Huntington's disease begins as a dysfunction in error feedback control. Nature. https://doi.org/10.1038/35000576.
Smith-Geater, C., Hernandez, S.J., Lim, R.G., Adam, M., Wu, J., Stocksdale, J.T., Wassie, B.T., Gold, M.P., Wang, K.Q., Miramontes, R., Kopan, L., Orellana, I., Joy, S., Kemp, P.J., Allen, N.D., Fraenkel, E., Thompson, L.M., 2020. Aberrant development corrected in adult-onset Huntington's disease iPSC-derived neuronal cultures via WNT Signaling modulation. Stem Cell Rep. https://doi.org/10.1016/j.stemcr.2020.01.015.
Strano, A., Tuck, E., Stubbs, V. E., & Livesey, F. J. (2020). Variable Outcomes in Neural Differentiation of Human PSCs Arise from Intrinsic Differences in Developmental Signaling Pathways. Cell Reports. https://doi.org/10.1016/j.celrep.2020.107732.
Thaler, J.P., Lee, S.K., Jurata, L.W., Gill, G.N., Pfaff, S.L., 2002. LIM factor Lhx3 contributes to the specification of motor neuron and interneuron identity through cell-type-specific protein-protein interactions. Cell. https://doi.org/10.1016/S0092-8674(02)00823-1.
Tremblay, R., Lee, S., Rudy, B., 2016. GABAergic interneurons in the Neocortex: from cellular properties to circuits. Neuron. https://doi.org/10.1016/j.neuron.2016.06.033.
Wang, R., Luo, Y., Ly, P.T.T., Cai, F., Zhou, W., Zou, H., Song, W., 2012. Sp1 regulates human Huntingtin gene expression. J. Mol. Neurosci. https://doi.org/10.1007/s12031-012-9739-z.
White, J.K., Auerbach, W., Duyao, M.P., Vonsattel, J.P., Gusella, J.F., Joyner, A.L., MacDonald, M.E., 1997. Huntington is required for neurogenesis and is not impaired by the Huntington's disease CAG expansion. Nat. Genet. https://doi.org/10.1038/ng1297-404.
Wyttenbach, A., 2001. Polyglutamine expansions cause decreased CRE-mediated transcription and early gene expression changes prior to cell death in an inducible cell model of Huntington's disease. Hum. Mol. Genet. https://doi.org/10.1093/hmg/10.17.1829.
Xie, Y., Hayden, M.R., Xu, B., 2010. BDNF overexpression in the forebrain rescues Huntington's disease phenotypes in YAC128 mice. J. Neurosci. https://doi.org/10.1523/JNEUROSCI.1637-10.2010.
Xu, X., Tay, Y., Sim, B., Yoon, S.-I., Huang, Y., Ooi, J., Utami, K.H., Ziaei, A., Ng, B., Radulescu, C., Low, D., Ng, A.Y.J., Loh, M., Venkatesh, B., Ginhoux, F., Augustine, G.J., Pouladi, M.A., 2017. Reversal of phenotypic abnormalities by CRISPR/Cas9-mediated gene correction in Huntington disease patient-derived induced pluripotent stem cells. Stem Cell Rep. 8 (3), 619–633. https://doi.org/10.1016/j.stemcr.2017.01.022.
Yaden, B.C., Garcia, M., Smith, T.P.L., Rhodes, S.J., 2006. Two promoters mediate transcription from the human LHX3 gene: involvement of nuclear factor I and specificity protein 1. Endocrinology. https://doi.org/10.1210/en.2005-0970.
Zhang, X.Q., Zhang, S.C., 2010. Differentiation of neural precursors and dopaminergic neurons from human embryonic stem cells. Methods Mol. Biol. https://doi.org/10.1007/978-1-60761-369-5_19. (Clifton, N.J.).
Zhang, X.H., Zheng, B., Gu, C., Fu, J.R., Wen, J.K., 2012. TGF-β1 downregulates AT1 receptor expression via PKC-δ-mediated Sp1 dissociation from KLF4 and smad-mediated PPAR-γ association with KLF4. Arterioscler. Thromb. Vasc. Biol. https://doi.org/10.1161/ATVBAHA.111.244962.
Zhang, L., Zhang, P., Wang, G., Zhang, H., Zhang, Y., Yu, Y., Zhang, M., Xiao, J., Crespo, P., Hell, J. W., Lin, L., Huganir, R. L., & Zhu, J. J. (2018). Ras and Rap Signal Bidirectional Synaptic Plasticity via Distinct Subcellular Microdomains. Neuron. https://doi.org/10.1016/j.neuron.2018.03.049.
Zuccato, C., Cattaneo, E., 2009. Brain-derived neurotrophic factor in neurodegenerative diseases. In Nature Reviews Neurology. https://doi.org/10.1038/nrneurol.2009.54.
Zuccato, C., Marullo, M., Vitali, B., Tarditi, A., Mariotti, C., Valenza, M., Lahiri, N., Wild, E.J., Sassone, J., Ciammola, A., Bachoud-Lèvi, A.C., Tabrizi, S.J., Di Donato, S., Cattaneo, E., 2011. Brain-derived neurotrophic factor in patients with Huntington's disease. PLoS One. https://doi.org/10.1371/journal.pone.0022966.